BIOETHANOL CATALYTIC PRE-REFORMING FOR RENEWABLE HYDROGEN PRODUCTION

Lappeenranta–Lahti University of Technology LUT

Master's thesis

Erasmus Mundus Joint Master Program in Sustainable Biomass and Bioproducts Engineering

2024

Jorge Andres Jimenez Llanos

Examiner(s): Inmaculada Moraleda Núñez, PhD. (Técnicas Reunidas S.A., Spain)
Manuel Salvador Carmona Franco, PhD. (UCLM university, Spain)
Kristian Melin, PhD. (LUT university, Finland)

ABSTRACT

Lappeenranta–Lahti University of Technology LUT

LUT School of Engineering Sciences

Erasmus Mundus Master Program Sustainable Biomass and Bioproducts Engineering

In co-operation with partner universities: Wrocław University of Science and Technology (Poland), Universidad de Castilla-La Mancha (Spain)

Jorge Andres Jimenez Llanos

Bioethanol Catalytic Pre-reforming for Renewable Hydrogen Production

Master's thesis

2024

60 pages, 43 figures, 18 tables and 0 appendices

Examiner(s): Inmaculada Moraleda Núñez, PhD. (Técnicas Reunidas S.A.), Manuel Salvador Carmona Franco, PhD. (UCLM), and Kristian Melin, PhD. (LUT)

Keywords: Green hydrogen, Pre-reforming, Stability, Catalytic activity, Reaction network.

The bioethanol catalytic steam pre-reforming stage in a steam reforming process is a sustainable and interesting method that breaks down alcohol molecules into simpler gas products which are later transformed into H_2. Técnicas Reunidas S.A. (TR) is a Spanish company that is currently working on validating commercial catalysts for multifuel pre-reformers as part of their ongoing low-carbon hydrogen production projects. This master's thesis assesses the technical feasibility of using bioethanol in the catalytic pre-reforming stage, employing a double-bed packed reactor under process conditions pre-defined by TR. A deep understanding of the performance of the pre-reformer was done with a DOE to determine the influence of the Gas Hourly Space Velocity (*GHSV*) in the range of (2500 to 4200) h^{-1} and Steam to Carbon ratio (*S/C*) between 2 and 3.5, followed by long-run stability tests and an exploratory reaction mechanistic study; the experimental work finished by validating the use of bioethanol at the selected best operating conditions. The results showed that *GHSV* and *S/C* had an effect on the H_2, CH_4 yield and their distribution in the overall composition profile; in contrast, these variables had no effect on the distribution of CO and CO_2. An interaction effect of both independent variables was statistically significant on the ethanol conversion, but showed no practical significance considering that all results were over 95%. The long-run test proved a stable performance in which 4200 h^{-1} and *S/C* 2 were selected as the best operating conditions. A reaction mechanism network was prosed to explain the composition evolution along the reactor bedding and the *T* profile. Finally, it was validated that bioethanol could be used in the catalytic pre-reforming stage at the best operating conditions by comparing the performance of the reactor to its performance while working with synthetic ethanol. The results of this work provided a detailed insight about the steady-state performance of the pre-reformer operating with synthetic ethanol and real 2nd generation bioethanol that will be used by TR for the future pilot-scale testing, scale up, and industrial commercialization of this technology.

GRAPHICAL ABSTRACT

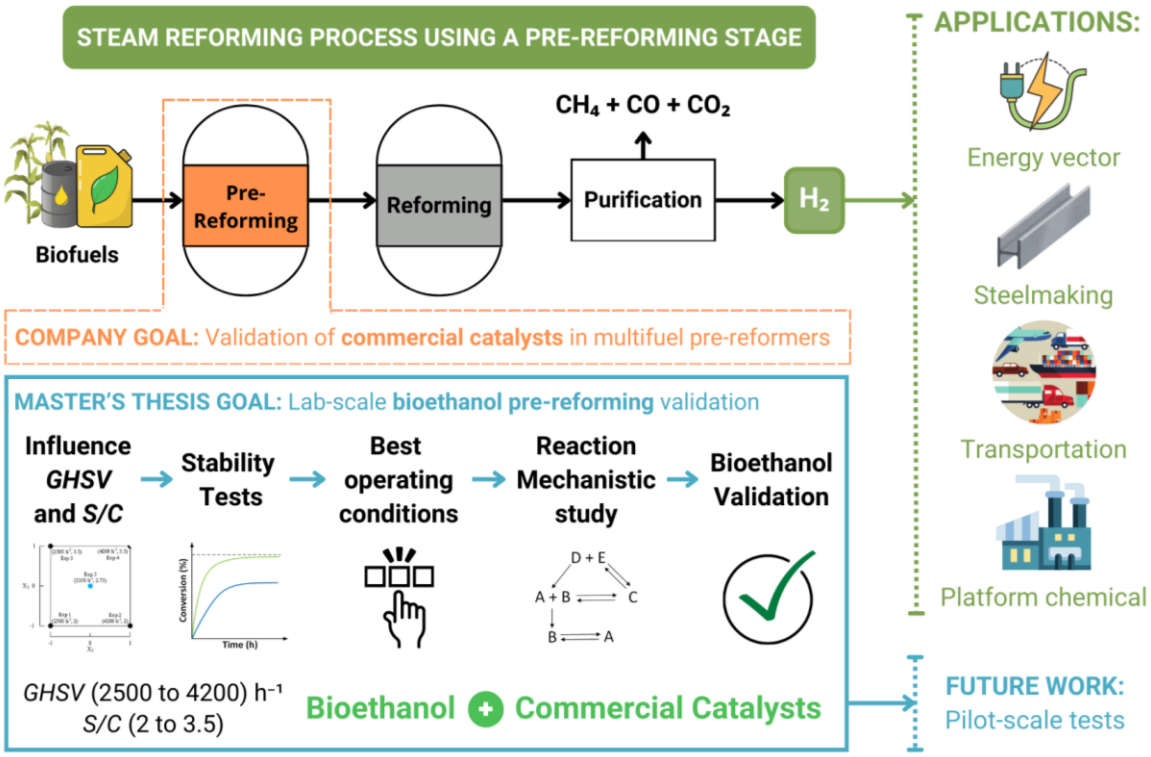

ACKNOWLEDGMENT

I would like to thank the SBBE consortium for believing in me before actually meeting me in person, for their hard work running this program, and showing that big projects can be achieved in a continuous state of improvement.

To my SBBE classmates, colleagues, and friends who became my family over this personal and professional growth journey; we faced the same challenges, and we overcame them working as team. I hope we can share many more meals in the future.

Thank you to every single person that I met at the three universities (WUST, UCLM, and LUT), professors, researchers, friends that were totally open to help and share their knowledge.

I recognize the role of the Técnicas Reunidas S.A. personnel, the supervisors, the laboratory co-workers and other people who trusted on my work and provide guidance during this thesis.

To my entire family who are the main pillars of my life, their support in person, by a phone call, a message, or their energy from heaven gave me the strength to keep moving forward.

Finally, I would like to thank myself, I proved that if a door closes, many others will open, to adapt fast, to keep a focus mindset, to my body for supporting the long study days. I don't expect to be perfect, but just to be a bit better every day.

SYMBOLS AND ABBREVIATIONS

Symbols and variables

	Name	Units
A	Surface area	mm^2
D	Diameter	mm
$\dot{F}$	Volumetric flowrate of species *j*	NL min^{-1} (N = 273.15 K, 0.1 MPa)
g-cat	Grams of catalyst	g
H	Height	mm
M	Mass	g
$\dot{M}$	Mass flowrate of species *j*	g min^{-1}
n	Moles of *j* species	mol-*j*
$\dot{N}$	Molar flowrate of species *j*	mol min^{-1}
P	Pressure / Gauge pressure	MPa / MPag
RI	Refraction index	-
R^2	Coefficient of determination	-
R^2_{adj}	Adjusted coefficient of determination	-
S/C	Steam to carbon ratio	mol-H_2O mol-C^{-1}
$STY\,j$	Space-time yield of j species	mmol-*j* h^{-1} g-cat^{-1}
S_{wall}	Surface of the reactor wall	mm^2
T	Temperature	K
t	Gas residence time	ms
V	Volume	mm^3
X	Conversion	%
X_{EtOH}	Ethanol conversion	%

Greek letters

	Name	Units
α	Level of significance	-
ε	Bed voidage	-
ρ	Density	g cm^{-3}
τ	Tortuosity	-
υ_e	Effective flow velocity	m s^{-1}
υ_l	Linear or superficial velocity	m s^{-1}
$\emptyset$	Sphericity	-

Subscripts and superscripts

	Name
b	Reactor packed bed
c	Catalyst
in	Inlet
j	Species
out	Outlet
e	Empty reactor
er	Effective reactor

Abbreviations

	Meaning
ANOVA	Analysis of variance
BF	Brown-Forsythe test
BioEtOH	Real 2nd generation bioethanol from fermentation
Cat / cat	Catalyst
DOE	Design of experiments
EtOH	Ethanol
GHG	Greenhouse gases
H0	Null hypothesis
H1	Alternative hypothesis
HE	Heat exchanger
KPI	Key performance indicators
n/a	Not applicable / Not available
n/c	Not considered
PR	Pre-reformer
SD	Standard deviation
SR	Steam reforming
SW	Shapiro-Wilk test
TR	Técnicas Reunidas S.A.

TABLE OF CONTENTS

INTRODUCTION **8**
1. BACKGROUND AND THEORETICAL DESCRIPTION **9**
1.1. Energy crisis and environmental challenges 9
1.2. Hydrogen economy 9
1.3. Color coding in hydrogen production 11
1.4. Bioethanol and H_2 production technologies 12
1.5. Pre-reforming 13
1.6. Current work and opportunities 15
1.7. Técnicas Reunidas S.A. and context of the master's project 16
2. AIM AND SCOPE **17**
3. METHODOLOGY **18**
3.1. Experimental setup 19
3.2. Reactor configuration and catalyst description 20
3.3. Process description and operating parameters 21
3.4. Analytical methods 21
3.4.1. Refractometry 21
3.4.2. Gas chromatography 22
3.5. Fluid dynamics and residence time 23
3.6. Design of experiments 24
3.6.1. Curvature test 25
3.6.2. Model fitting 26
3.7. Initial long-run stability test with synthetic ethanol 26
3.8. Selection of the best operating conditions based on the long stability results 26
3.9. Exploratory reaction mechanistic study 27
3.10. Short-run test using Bioethanol 28
3.11. Long-run test using Bioethanol 28
3.12. Aspen HYSYS® simulation 28
4. RESULTS AND DISCUSSION **30**
4.1. Catalytic performance of the pre-reformer at different operating conditions 30
4.1.1. DOE: Influence of GHSV and S/C 30
4.1.2. Initial long run stability tests 35
4.1.3. Selection of the best operating conditions 42
4.2. Exploratory reaction mechanistic study 43
4.3. Experimental performance of the pre-reformer using Bioethanol 49
4.3.1. Bioethanol short-run test 49

4.3.2. Bioethanol long-run stability test 51
CONCLUSIONS **53**
RECOMMENDATIONS FOR FUTURE WORK **54**
REFERENCES **55**
LIST OF TABLES **59**
LIST OF FIGURES **60**

CONFIDENTIAL DISCLOSURE AGREEMENT

The student conducted his thesis at the Técnicas Reunidas S.A. Laboratory at the University of Castilla-La Mancha in Ciudad Real, Spain, and signed a confidentiality agreement. This agreement required him to keep all technical, legal, economic, and organizational information confidential, particularly details about the catalyst, reactor dimensions, and other relevant operation conditions. He agreed not to disclose or use any confidential information without prior consent from Técnicas Reunidas S.A., even after completing his thesis. This included maintaining the secrecy of technical, contractual, business, commercial, licensing, and patent information. He also had to handle any personal data according to the company's instructions, ensuring that all information remained secure and undisclosed to unauthorized parties.

INTRODUCTION

The world is undergoing an energetic global crisis that will increase the global energy demand from 630 EJ in 2022 to 670 EJ by 2030, from which around 80% of the demand is expected to be covered with fossil fuels; thus, increasing the emissions of CO_2 and accelerating global warming [1]. Transitioning to sustainable energy sources and carbon-zero technologies is essential to overcome these challenges supported by new energetic and environmental policies like the European Green Deal, which aims to reduce by 55% by 2030 and be the first climate-neutral continent by 2050 [2]. Although it is visionary, several scenarios forecast a decrease in fossil fuel participation in the energy matrix ranging from (15 to 45)% between 2030 and 2050 [1].

The concept of a "H_2 economy" has gained a significant attention as H_2 is a versatile energy vector and platform chemical with a wide range of applications [3]; traditionally, it has been used as a feedstock to produce direct reduced iron, methanol, and ammonia; recent potential new applications include transportation, power generation and upgrading of biofuels [4]. In 2022, global H_2 usage was 95 million tons, representing an increase of 3% compared to 2021 [4]; yet 95% of that H_2 was obtained from fossil fuels, releasing 830 million tons of CO_2 per year [5]. The implementation of the H_2 economy is rapidly evolving by prioritizing green H_2 production; several countries, such as Colombia, Poland, Spain, and Finland already have roadmaps and strategies to integrate H_2 into their current energy matrix [6–9].

Some approaches for producing H_2 include electrochemical, biological, thermochemical, and reforming methods [10–12]. Among them, catalytic steam reforming (SR) is currently the best available technology that represents 48% of the total H_2 produced [5]. Recently, the use of biofuels such as bioethanol (BioEtOH) has gained attraction as an alternative to the use of fossil fuels for SR processes considering their renewable nature and lower carbon footprint [13]. However, direct SR of BioEtOH has been proven to be challenging due to the formation of coke that can poison the catalyst lowering the yield and stability of the reformer over time [14].

A steam pre-reforming reactor converts higher hydrocarbons and biofuels like BioEtOH into a mixture of mainly H_2, CH_4, and carbon oxides like CO and CO_2 emerging as a possible solution to prevent coke formation in a subsequent reforming stage. The use of a pre-reformer (PR) could further enhance the efficiency and sustainability of BioEtOH-based SR processes and can be easily integrated into the existing SR infrastructure [15]. BioEtOH pre-reforming is an area of active research and development, focusing on understanding the main reaction routes, controlling important variables such as *T*, *P*, catalyst properties, and addressing the influence of impurities [16]; however, more research is needed before its fully industrial application.

Técnicas Reunidas S.A. (TR) from Spain through the specialized division of heat transfer (TR-Tecnical) is currently validating the use of commercial catalysts to develop modular multifuel pre-reforming reactors aiming to scale up and commercialize this technology; thus, taking a step further to a net zero carbon emission world. This master's thesis work was developed in the TR testing lab in Ciudad Real to assess the technical feasibility of using BioEtOH in the pre-reforming stage of a SR process for H_2 production using a selected combination of catalysts and process conditions. First, this report discusses the steady-state catalytic performance of the PR at different operating conditions using synthetic ethanol (EtOH); later, the catalytic performance of the PR is explained based on an initial exploratory reaction mechanistic study; finally, the use of real BioEtOH in the pre-reforming reactor is assessed while working at the best selected operating conditions.

1. BACKGROUND AND THEORETICAL DESCRIPTION

This section provides the background and theoretical knowledge necessary to understand the context and objectives of this master's thesis.

1.1. Energy crisis and environmental challenges

The world has always been in a continuous state of change, and each period of time has had its own challenges. Today, climate change and global warming have been widely identified as the principal threats to break the fragile global equilibrium [14]. Thanks to industrialization and more demanding lifestyles [17], the energy demand has increased over the decades and is expected to keep increasing by 56% between 2010 and 2040 [3]; of which around 80% is expected to be covered by fossil fuels, increasing pollutants and emissions of greenhouse gases (GHG) like CO_2 and intensifying not only global warming [1, 3] but also negative impacts on human well-being such as respiratory and cardiovascular effects due to extreme weather conditions in addition to mental effects, malnutrition, and food safety security [3]. Additionally, fossil fuel exhaustion combined with other complex pressing geopolitical and macroeconomic challenges are pushing to transform the energy scenario urgently [1].

A transition to carbon neutral renewable energy resources is the principal path to remediate global warming effects and to achieve sustainable development [17]. Several multilateral agreements such as the 2019 European Green Deal have given H_2 the outstanding potential to become the most competitive and feasible clean fuel of the future by developing the denominated "H_2 economy" [2, 14].

1.2. Hydrogen economy

H_2 is the most abundant element in the universe, it is an odorless, colorless, and highly flammable gas, mostly found in a variety of chemical compounds such as H_2O and hydrocarbons such as CH_4 but rarely found in its pure form [3]. It has emerged as a functional clean energy carrier with the potential to decarbonize various sectors since its energy output is 2.75 times higher compared to other fossil fuels; also, its combustion only produces water without any other pollutants [17]. Its major attractiveness lies in the ability to be produced from diverse energy sources and its applications in multiple industries, playing a crucial role for a sustainable the energy transition [18].

H_2 economy relies on its dual role as a platform chemical and a possible energy vector. As an energy vector, H_2 can store and deliver energy without producing GHG emissions. As a platform chemical, it is utilized in many industries, like as a reducing agent in the refining and steel industry, as a feedstock in chemical manufacturing to produce ammonia, methanol, and synthetic fuels, thereby contributing to the decarbonization of the chemical industry [14, 18].

Regardless of its benefits and applications, widespread adoption of H_2 has been limited, due to some obstacles. Advanced technologies are needed for the effective storage and transportation of clean H_2, which increases production costs. Moreover, several locations are still under infrastructure development for its use in applications such as transportation, hindering maturity commercially [18]. Despite H_2 is considered a clean fuel, the production processes to obtain it are known to release high amounts of carbon emissions [14]; for

instance, currently about 95% of the total produced is obtained from non-renewable fossil sources such as SR of natural gas and coal gasification [5, 17].

A comprehensive roadmap is essential for a broader implementation of H_2 technologies. This includes establishing the infrastructure necessary for its production, storing, and distribution as well as developing new policies and other incentives to encourage its use. In Europe, countries like Spain, Poland, and Finland are making significant initiatives for their H_2 strategies. Spain's 2021 Energy Policy Review stated the goal to achieve net zero emissions by 2050 aiming for 97% renewable energy in the total energy mix relying on the use of H_2 for transportation, industrial processes, and energy storage [7]. Poland exposed in 2021 the goal to develop H_2 technology to support its decarbonization targets for 2030, focusing on green H_2 production through renewable energy sources and reduce its heavy dependence on coal, especially in sectors such as transportation, industry, and power generation [9]. The Finnish government published in November 2020 the National H_2 Roadmap stablishing the ambitious initiative to achieve carbon neutrality by 2025 and reducing GHG emissions by 90% in 2050 while commercializing new energy technologies, specially aiming for low-carbon H_2 industrial usage by 2030 [6]. In Latin America, Colombia efforts are focused explore H_2 production by using its abundant biomass resources and energy sources like wind, solar, and geothermal, this aiming to cut GHG emissions by 51% by 2030 [8].

The global status of H_2 use and implementation varies by region. Figure 1 displays a dynamic global landscape for H_2 consumption and project development based on H_2 technologies. China stands out as the largest consumer with nearly 30% of the global consumption. The United States follows with 17% of consumption, quite similar to the whole Middle East. Europe has seen a significant decline in H_2 use, with a drop of nearly 6% in 2022 compared to 2021 due to reduced chemical industry activity and rising natural gas prices intensified mostly by geopolitical factors. However, Europe and Australia account for about 50% of new H_2 projects, with increasing development also emerging in the United States, Latin America, China, Africa, and India. This pattern indicates a rising global interest in H_2 technology, even as Europe faces declines in its consumption as mentioned [4].

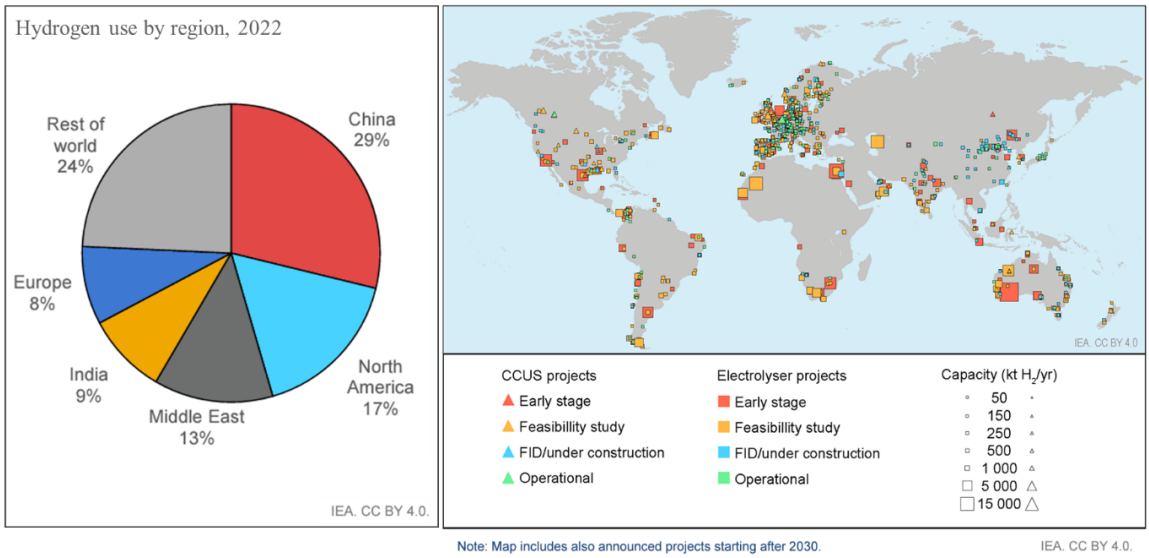

Figure 1. *H_2 use and summary map of announced low-emission hydrogen production projects by region. Source:*[4]

1.3. Color coding in hydrogen production

Color codes are frequently used in environmental science and engineering to indicate the degree of purity of a particular resource. Thus, H_2 classification was developed to help consumers, policymakers, and project developers to assess the advantages of several H_2 generation methods in the context of a future powered by renewable energy sources [19]. The main colors used for H_2 production are based on feedstock, production technology, source of energy, and environmental impacts as seen in Figure 2; although there are other colors like turquoise, yellow, red, and white. **In the context of this thesis work, H_2 will be produced from a biomass-based feedstock which is BioEtOH using a thermochemical process called steam pre-reforming; therefore, green H_2 would be the corresponding color**.

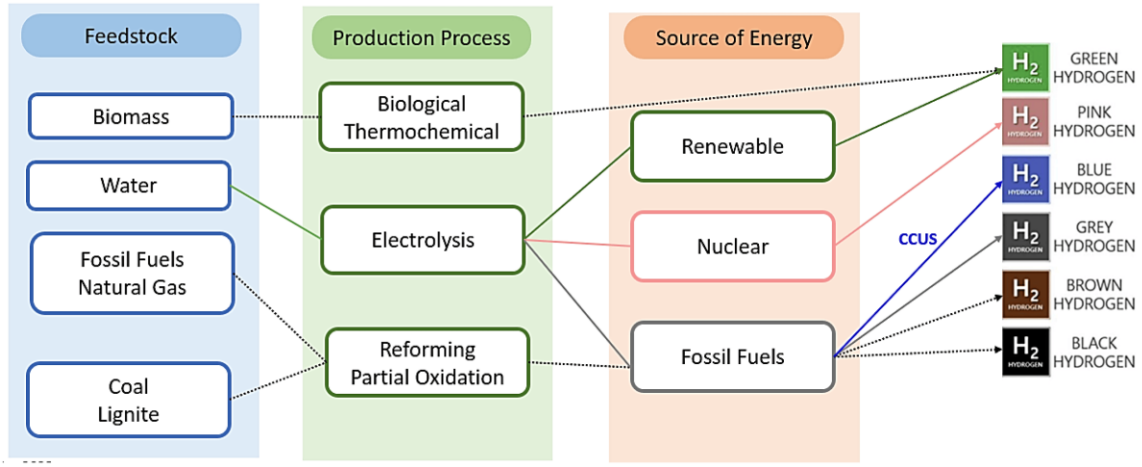

***Figure 2**. Classification of H_2 production based on colors. Source:* [20]

Figure 3 shows the results of a bibliographic review conducted by [18] using the Web of Science and Scopus databases where the author mapped studies related to the techno-economic evaluation of H_2 production from 1950 to 2023 based on color coding and measured by the number of research results. Green H_2 shows the highest interest with 33,984 results, reflecting a significant focus on environmentally friendly methods. It is followed by blue H_2, which involves natural gas with carbon capture and storage with 22,460 results. This is likely due to blue's H_2 role as a transitional technology since it serves as a bridge between the current reliance on fossil fuel and the reduction in carbon emissions compared to the traditional methods. White H_2, which is the naturally occurring formation of H_2 and black H_2 both had around 10,000 results highlighting just a moderate interest. This distribution displays a clear preference for sustainable and lower-emission technologies in the H_2 production research [18].

It is worth mention that as technologies have been created and different raw materials have been utilized, classifying H_2 has become increasingly complex due to the various nuances and definitions proposed by different authors. To standardize the classification and improve economic forecasting, recent studies and projects have aimed to introduce a new classification for the H_2 obtained. For example, in a research made by [21], the authors affirmed that there is not a unified commonly agreed color code for several technologies' pathways having a misleading concept among researchers; they proposed a visual representation based on a 3-colour depending on the CO_2 emitted in the production process. Other initiatives like the CertifHy project, aimed to create a robust certification scheme for

green and low-carbon H_2 in Europe, defining and certifying it based on its carbon footprint and production methods. CertifHy Green H_2 is characterized by being originated from renewable sources and possesses a GHG balance less than 60% of the H_2 production through state-of-the-art SR of natural gas, which has a benchmark GHG footprint of 94 g CO_2-eq MJ-H_2^{-1} [19]. Finally, the TÜV Rheinland Standard H2.21 specifies even stricter limits with a GHG reduction threshold of 70% based on the same benchmark value as the CertifHy project [22]. In conclusion, H_2 classification is evolving as H_2 technologies emerge.

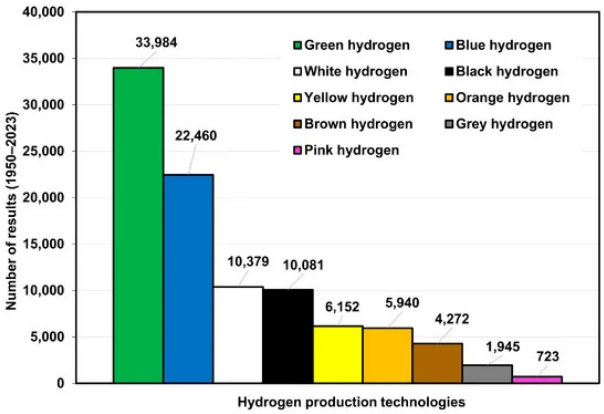

***Figure 3**. Bibliographic review of techno-economic evaluation of H_2 production from 1950 to 2023 based on color coding. Source:* [18]

1.4. Bioethanol and H_2 production technologies

H_2 can be produced through various processes, Figure 4 provides an overview of the most common methods utilized, where they are grouped by the input source, either renewable or from fossil fuels and each of them directed to a specific range of applications.

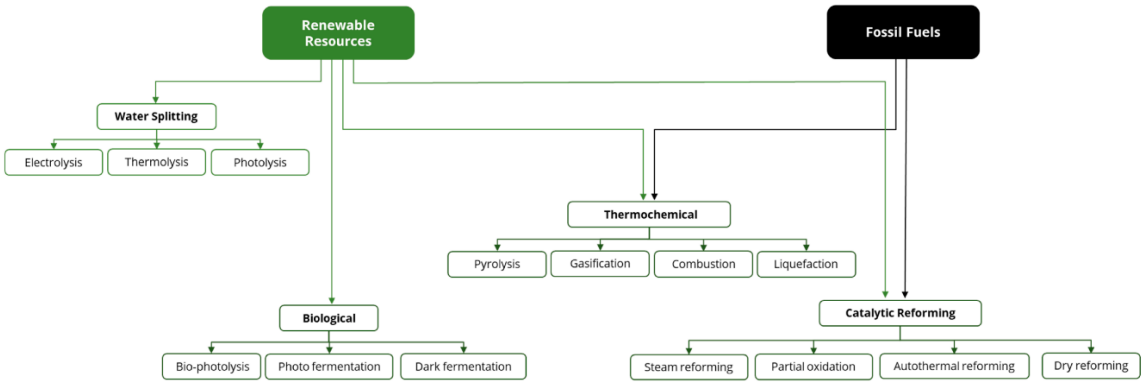

***Figure 4.** Scheme of H_2 production technologies and their feedstock. Source:* [12]

Among these technologies, catalytic reforming processes have played a key role for H_2 production due to their efficiency, cost-effectiveness, and its adaptation ability to industrial environments. This category includes methods such as SR, partial oxidation, autothermal reforming, and dry reforming, responsible to convert hydrocarbons and other compounds along with steam or O_2 into H_2, CO and CO_2.

As mentioned before, SR reforming stands out being the most studied and widely used method for large-scale operation, due to its cost-effectiveness. It supplies over 48% of global

H_2 demand; however, a significant amount of CO_2 is emitted using this technology because it uses majority natural gas, thereby undermining the benefit of employing H_2 as a clean energy source [12]. Thus, green energy sources for reforming process and improved catalysts for higher conversion and stability are needed.

The primary raw materials for H_2 production through reforming processes include mostly natural gas and CH_4 reacting with H_2O and O_2 via several reaction pathways. Moreover, studies have been performed employing other compounds such as methanol, EtOH, glycerol, acetic acid, and toluene to investigate their effectiveness and viability [12]

BioEtOH stands out from the rest due to its renewable nature and higher energy density compared to conventional hydrocarbons like CH_4 and natural gas, proving to be a great and more sustainable energy solution [14, 23]. This compound, when derived from biomass, offers a more sustainable alternative over the cited raw materials, decreasing the reliance on fossil fuels and reducing GHG emissions more effectively than synthetic EtOH or other hydrocarbons, becoming a strong option for cleaner H_2 production [17]. Additionally, it is sulfur-free, easy to transport, decomposes easily, and produces more H_2 than methanol [24]. Based on the used catalytic reforming methods, BioEtOH can undergo several reaction pathways (Rx. 1 to Rx. 4):

Steam reforming:	$C_2H_5OH + 3H_2O \leftrightarrows 2CO_2 + 6H_2$	Rx. 1
Partial oxidation	$C_2H_5OH + \frac{3}{2}O_2 \leftrightarrows 2CO_2 + 3H_2$	Rx. 2
Dry reforming	$C_2H_5OH + CO_2 \leftrightarrows 3CO + 3H_2$	Rx. 3
Autothermal reforming	$C_2H_5OH + H_2O + O_2 \leftrightarrows 2CO_2 + 4H_2$	Rx. 4

The review on H_2 production from BioEtOH made by [14] highlights its potential as a sustainable and renewable source through SR and other catalytic processes. Key findings show that BioEtOH in a range of purity levels (50 to 90%vol.), can effectively produce H_2 with high conversion rates, demonstrating the feasibility of using even less purified BioEtOH. The optimal conditions for H_2 production were identified, including *S/C* (3 to 5) and *T* around (773 to 873) K for SR. Additionally, the integration of BioEtOH reforming with fuel cells for combined heat and power generation emphasizes its potential to support a circular economy by utilizing the CO_2 produced during the process for further catalytic conversion, thus enhancing the overall process efficiency and making it even more sustainable.

Nevertheless, the big backlash of the direct SR of BioEtOH is the favorability towards coke forming reactions, especially at high *T* in the SR process; additionally, there are none commercially available catalysts intended for this use yet; thus, creating an additional challenge facing a massive industrial application. To avoid coke-formation inside the main reformer reactor, a PR can be installed before the main stage of a SR process to break down the BioEtOH into gaseous products that can be further easily converted to H_2.

1.5. Pre-reforming

Pre-reforming has emerged as an essential stage in the efficient reforming of biofuels and higher hydrocarbons for H_2 production [25]. **The main goal of this stage is the conversion of heavier hydrocarbons and fuels into lighter, more manageable molecules like H_2, CH_4, and carbon oxides which later can be further converted into a H_2-rich stream in**

the main reforming stage of the process. By breaking down complex hydrocarbons, pre-reforming aids smoother reactions in the subsequent reforming processes, leading to higher H_2 yields, improved catalyst performance and low coke formation inside the tubes of the main reformer. This approach not only optimizes its production but also contributes to the reduction of by-products, making it a crucial component in the development of sustainable technologies [15].

Figure 5 shows a typical SR process with a PR unit installed before the main reforming stage; later H_2 is purified by a water-gas shift reactor and a pressure swing adsorption unit. The pre-reforming reactor typically operates at (673 to 800) K with the same catalyst than the SR [15]. The pre-reforming stage helps to prevent coke formation and catalyst deactivation in the main reformer. Additionally, by conducting BioEtOH conversion in the PR, the system benefits from a simpler and more manageable catalyst replacement process. Moreover, the production of CH_4, CO, or CO_2 in the pre-reforming stage does not bring negative effects as these compounds can be subsequently converted to H_2 in the main stage of reforming. This configuration offers the flexibility to switch between renewable and fossil feedstocks based on availability and cost, enhancing the overall efficiency, safety, and operational reliability of the H_2 production process [15].

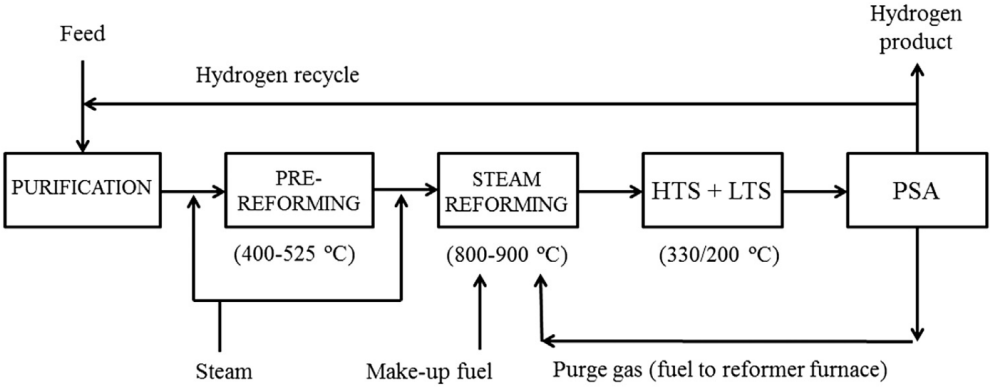

Figure 5. *Scheme of a SR process using a pre-reforming reactor. Source:* [25]

In the simplest way, a pre-reforming reactor can be described by three reactions using BioEtOH as an example [15], the first one is the SR described in Rx. 1, the other two correspond a CH_4 forming reaction and the conversion of CO into CO_2 (Rx. 5 and Rx. 6).

$$\text{Methanation:} \quad CO + 3H_2 \leftrightarrows CH_4 + H_2O \qquad \text{Rx. 5}$$

$$\text{Water-gas shift:} \quad CO + H_2O \rightarrow CO_2 + H_2 \qquad \text{Rx. 6}$$

Nevertheless, the BioEtOH pre-reforming catalytic system is much more complex than three reactions [26]. In a similar way as in the direct SR process, BioEtOH can follow several reaction pathways depending on many factors such as *T*, *P*, and catalyst properties [27]. Figure 6 shows a proposed more detailed reaction network in which BioEtOH breaks down through several mechanisms like dehydrogenation, dehydration, decomposition, and direct SR which are followed by the mentioned water-gas-shift and methanation reactions [24]. Many intermediates can be formed like acetaldehyde, ethylene, and ethane. Coke-forming reactions like Boudouard or CH_4 cracking are undesired since they can poison the catalyst, resulting in low performance and reduced lifespan of the catalyst. Although there have been common agreements about the types of reactions; there are still many unanswered questions about the reaction mechanism of BioEtOH pre-reforming depending especially on the types

of catalyst used. They should be theoretically and experimentally analyzed to proper optimize the catalytic reactors [23, 28]

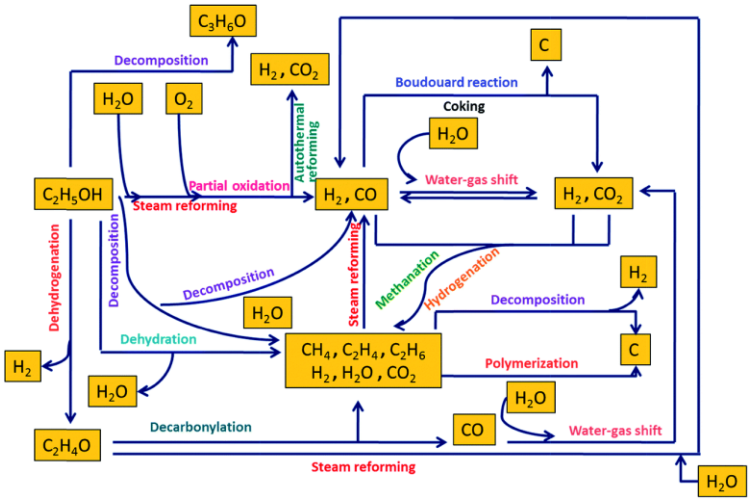

Figure 6. *Possible reaction pathways for the BioEtOH pre-reforming process. Source:* [29]

1.6. Current work and opportunities

Figure 7 shows the historical results of a bibliographic study conducted by [12] about the technical-economic viability of H_2 production publications up to 2022. It is evident the increased interest in the area and shows a strong willingness to create an H_2 economy. 2022 peaked with 29% of the total 977 publications made in the last five decades, suggesting that there is a favorable environment for the research and industrial implementation of H_2 technologies [12].

This study also concluded that 33% of the publications were related to "water splitting", the category "thermochemistry" represented 31% of the publications, and the category "catalytic reforming" represented 19% of the publications in which the subcategory "steam reforming" represented 15% of the publications. Therefore, more research about SR is needed to promote the use of this technology at industrial scale, especially in the steam pre-reforming of biofuels like BioEtOH. The company TR is aware of this gap and currently is working for the future commercialization of this technology.

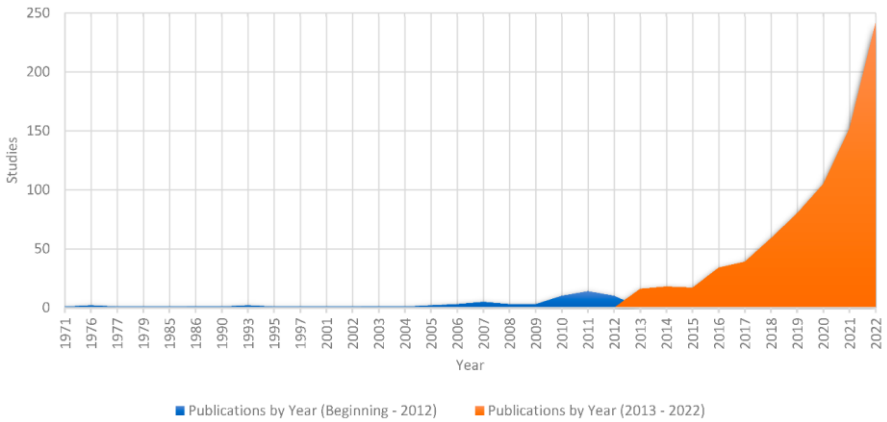

Figure 7. *Scheme of a SR process using a pre-reforming reactor. Source:* [12]

1.7. Técnicas Reunidas S.A. and context of the master's project

TR is a renowned Spanish engineering, procurement, and construction company that offers sustainable solutions for the oil and gas, power generation, and industrial plants sectors. TR was founded in 1959 with a primary focus on the design and construction of refineries, petrochemical plants, gas processing facilities, and power plants. In recent years, TR has shifted its focus towards the energy transition, with a growing portfolio of projects related to low-carbon technologies. Nowadays, TR has established its position as a global leader company in business areas related to natural gas, petrochemistry, refining, and low-carbon technologies [30]. To keep its position in the global market, TR always foresees the future and adapts to new challenges with strategies like the SALTA program, which seeks a new internal model of organization based on the creation of five business units (Engineering & services, Energy, North America, Europe & the World, and Middle east) [31].

In its 65-year history, TR has designed and constructed over 1000 industrial plants located in more than 50 countries and currently there are 30 ongoing projects in 20 countries [30]. Among these, The SHINE-FLEET project aims to develop technological solutions based on H_2 for the smart and sustainable mobility of heavy-duty fleets; TR works on developing a compact and modular generation system to produce *in-situ* renewable H_2 [32]. The ZEPPELIN project aims to develop new green and flexible technologies alternative to electrolysis to produce and store H_2 based on the valorization of waste and by-products from different sectors [33].

To accomplish these goals, TR has been validating at laboratory scale the use of commercial catalysts in multifuel reactors especially for the use of BioEtOH in industrial processes; as a result, it is expected to reduce the energy consumption and steam demand compared to current technologies. This validation is important because nowadays there are no commercial catalysts being sold exclusively for the steam pre-reforming of BioEtOH; therefore, this new innovative industrial process must be achieved by challenging the current limits of the best available technologies and expanding their boundaries to reach new applications.

2. AIM AND SCOPE

A step-by-step laboratory validation is imperative to determine the viability of this technology before moving into large-scale operations. Likewise, based on the current trend to promote the use of PRs as precursors for green H_2 production in SR processes and the goals the company set for the SHINE-FLEET and ZEPPELIN projects; TR proposed through its testing laboratory located at the Universidad de Castilla-La Mancha a methodologic understanding of a PR performance using synthetic EtOH before moving into the evaluation of the performance working with BioEtOH employing process parameters defined by its previous expertise and studies in the field. Considering this context, **the main objective of this master's thesis was set to assess the technical feasibility of using real BioEtOH in the catalytic pre-reforming stage of a steam reforming process to produce H_2 using the catalysts, reactor configuration and process conditions previously defined by the company TR.**

Three specific objectives were established to reach the main goal of this work:

- To study the steady-state catalytic performance of the PR at different operating conditions using synthetic EtOH.
- To explain the steady-state catalytic performance of the PR based on an exploratory reaction mechanistic study at selected operating conditions
- To compare the steady-state catalytic performance of the PR when working with EtOH and BioEtOH at selected operating conditions

The successful completion of this work would have a significant impact, especially from an industrial perspective regarding the process of scaling up of green technologies and their future commercialization. In the first place, these results would serve TR to achieve some of the goals set for the SHINE-FLEET and ZEPPELIN projects; also, the results pretend to validate the use of BioEtOH at lab scale in a steam pre-reforming process and select the best suitable conditions that later will serve as input for pilot-scale validations. The understanding of the steady-state performance and the possible reaction network of the PR will provide first-hand information for further optimization and scale up studies. Finally, this work represents one more step towards the implementation at the industrial scale of pre-reforming units based on biofuels like BioEtOH that can be integrated to already installed SR technologies; thus, contributing to the goal of becoming a carbon neutral world by 2050.

3. METHODOLOGY

The methodology section outlines the experimental procedures and analytical techniques employed to achieve the main objective of this work. Table 1 to Table 4 summarizes the chemicals, reactants, materials, equipment, and software used to perform the methodology, they were mentioned directly or indirectly in the procedure description. Chemicals and reactants were used without further purification.

***Table 1**. Summary of chemicals and reactants used in the methodology*

Material	Composition	Purity	Company	Origin
Ar gas	Ar	≥99.999% vol.	AL Air Liquide España, S.A.	Spain
BioEtOH	C_2H_6O	EtOH 99.641% wt.	n/a[a]	n/a[a]
EtOH	C_2H_6O	(96.0 to 96.6)% vol.	PanReac AppliChem	Spain
H gas	H_2	≥99.999% vol.	AL Air Liquide España, S.A.	Spain
He gas	He	≥99.999% vol.	AL Air Liquide España, S.A.	Spain
N gas	N_2	≥99.999% vol.	AL Air Liquide España, S.A.	Spain
Type I water	H_2O	Conductivity 0.056 µS cm^{-1}	Water generator in Table 3	Spain

[a] Detailed information could not be disclosed as a result of a confidentiality agreement

***Table 2**. Summary of other materials used in the methodology*

Material[a]	Composition	Company[a]	Origin[a]
Cat A	Supported metallic active phase[b]	n/a	n/a
Cat B	Supported metallic active phase[b]	n/a	n/a

[a] Detailed information could not be disclosed as a result of a confidentiality agreement

[b] Both catalysts had the same type of support but different metallic active phase

***Table 3**. Summary of the equipment used in the methodology*

Equipment	Company	Model	Other information
Gas chromatograph	Agilent Technologies	Process µGC	n/a[a]
Microactivity-Effi	PID Eng&Tech	MAE16	n/a[a]
HPLC pump	Gilson	307	Flowrate (0.02 to 5) cm^{-3} min^{-1}
Reactor	n/a[b]	n/a[b]	Stainless steel, TR own design
Refractometer	Atago CO., LTD.	RX-5000	Refraction index ±0.00004
Type I water generator	Millipore Corporation	Milli-Q Gradient A 10	Water quality compiled with ASTM Type I Reagent Grade Water

[a] Not applicable

[b] Information could not be disclosed as a result of a confidentiality agreement

***Table 4**. Summary of software used in the methodology*

Software name	Version	Year	Company	Location
Aspen HYSYS®	12.1	2021	Aspen Technology Inc.	Bedford, MA, USA
Statistica®	13.0	2017	TIBCO Software Inc.	Tulsa, OK, USA

A standardized criterium was defined to have a consistency on how the data was presented along this report; hence, the round-up of values were done following the indications of the ASTM E29-22 standard [34]; while the number of significant digits was chosen according

to the recommendations presented by [35] summarized in Table 5; therefore, the number of decimals and significant digits could change according to the significance for each reported variable.

***Table 5**. Criterium used to define the number of significant digits for the reported values*

Summary statistic	Reporting
Mean	Use enough decimal places to give SD two significant digits
SD, CV	One or two significant digits
R^2, R^2_{adj}	Use one or two decimal places
R	One or two decimal places or more when close to ±1
Test statistics: t, F	Up to one decimal place and up to two significant digits
p-value	Rounded up to one significant digit, the lower limit may be as small as 0.001 depending on the significance

Source: Table 1 published in [35]

3.1. Experimental setup

The main setup used to perform the present methodology consisted of a Microactivity-Effi MAE16 equipment with various peripheral units that conformed an integrated, modular, compact, fully-automated laboratory system that allowed to conduct experiments under controlled conditions of T, P, and feed composition to systematically investigate the performance of a catalytic reactor for the EtOH steam pre-reforming conversion into a H_2 and CH_4-rich gas. The relevant peripheral units and internal components of the setup are shown in Figure 8.

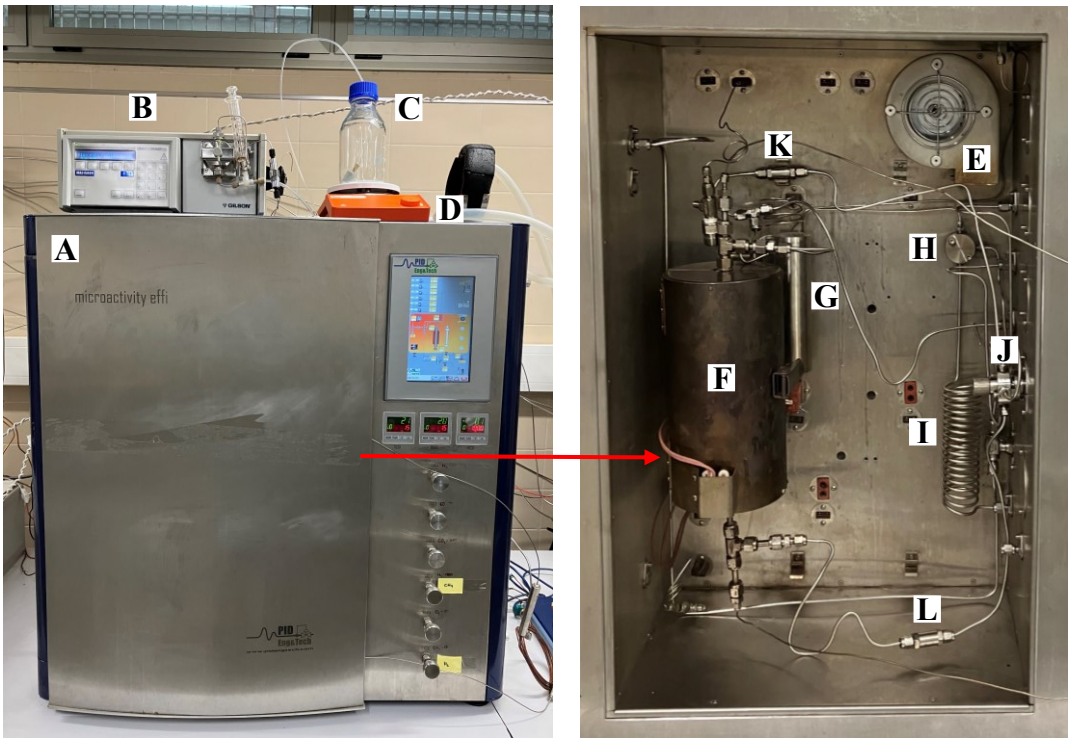

***Figure 8**. Experimental setup*

A) Microactivity-Effi MAE16, B) HPLC liquid pump, C) Liquid storage, D) Magnetic stirrer, E) Hot box fan, F) Reactor + Furnace, G) Evaporator, H) Gas/vapor mixer, I) Gas heat exchanger, J) Multiway rotary valve, K) Inlet filter, L) Outlet filter. Source: Author

The liquid inlet stream is pumped by the HPLC pump into the Microactivity-Effi MAE16 equipment passing through a check valve and subsequently being evaporated; other gases like H_2 and N_2 are heated in the hot box heat exchanger in another stream that later is mixed with the vapor through a gas/vapor mixer to obtain a unique homogeneous stream. Next, the resulting stream flows through a multiway rotary valve, a filter to prevent the entry of any possible particles that could harm the operation of the equipment, and finally heated to ensure the T needed at the inlet of the reactor.

After the pre-reforming reactions occurred inside the reactor, the wet gas product stream passes through another filter that catches small particles of broken catalyst and possible coke formed inside. Later, it passes through a Peltier cell at 285 K to condensate unreacted EtOH and water as liquid effluent giving out a dry gas product stream. Finally, the total $\dot{F}^{out}$ of the product gas stream is measured using a gas flowmeter and its composition quantified using an online gas chromatograph. Data regarding the operating conditions at each stage of the process was monitored during the experiments and collected automatically on a desktop computer. The process diagram of the described procedure is shown in Figure 9.

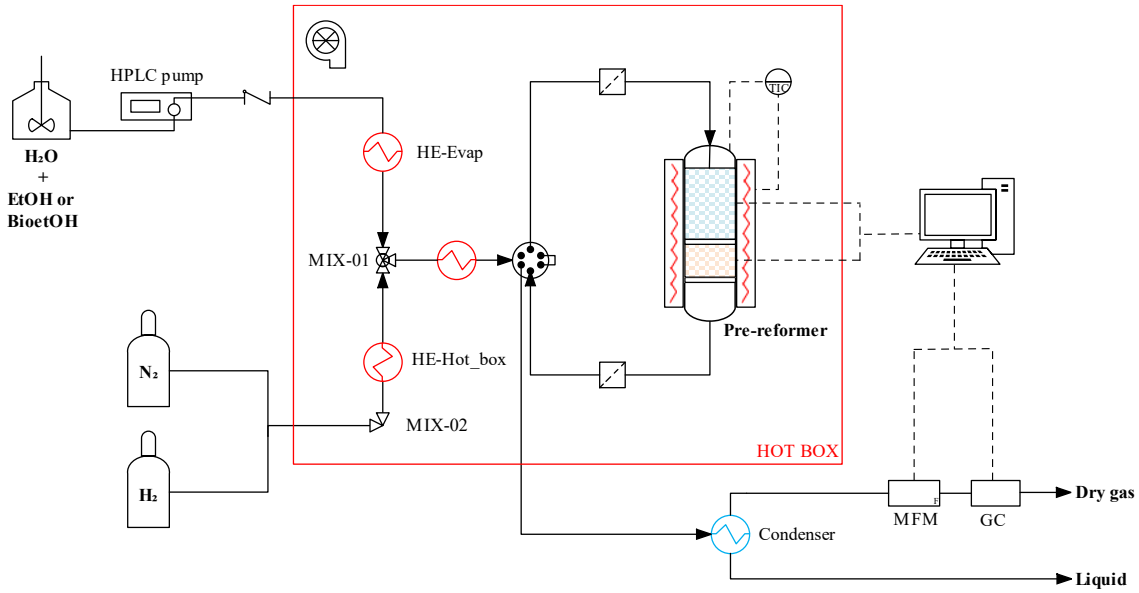

Figure 9. *Process diagram of the experimental setup. Source: Author*

3.2. Reactor configuration and catalyst description

A stainless-steel vessel that TR designed and built for this process was used as the pre-reforming reactor with defined H_b and D_b. For all the experiments, Cat A composed the first 60% of the V_b while the other 40% was Cat B. A 0.07 mm tick stainless steel mesh was placed between the Cat A and the Cat B sections inside the vessel; the bottom part had a quartz support to hold the reactor bedding. Two type K four-channel thermocouples were placed through the center of the reactor making eight measuring points to register the T alongside the packed bed for each experiment. The reactor was surrounded by an electric furnace to provide the energy required to promote the catalytic reactions. The pre-reforming reactor configuration is shown in Figure 10.

Cat A and Cat B had the same type of support but different metallic active phases. Their D_c and H_c were measured in the laboratory to determine other physical properties needed for

the calculations. The catalysts were activated before each experiment following the recommendations of the manufacturer. The detailed catalyst's composition, properties and activation procedures could not be disclosed due to a confidentiality agreement; however, they will be recalled in this report to explain some results.

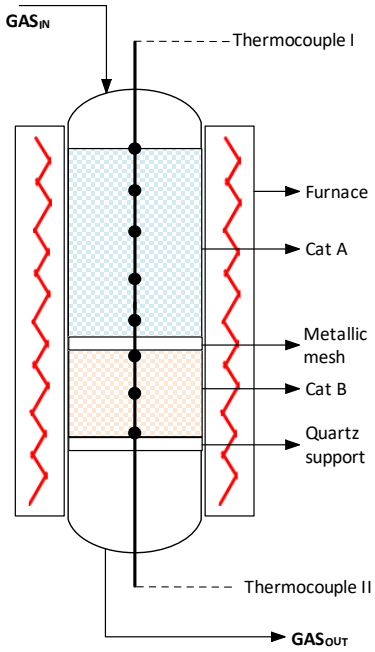

Figure 10. *Reactor configuration for the EtOH steam pre-reforming using the Microactivity-Effi equipment setup. Source: Author*

3.3. Process description and operating parameters

Reagent grade type I water produced *in-situ* using the Milli-Q water generator and synthetic EtOH or real BioEtOH were mixed in a vessel using a magnetic stirrer. The composition and flowrate of the liquid stream were adjusted depending on the needed process conditions of *S/C* (2 to 3.5) and *GHSV* (2500 to 4200) h^{-1}.

For all the experiments, a sufficient gas flowrate was set to obtain 3 %vol. H_2 and 5 %vol. N_2 at the inlet of the reactor, the evaporator was set to 623 K while the hot box operated at 453 K, the inlet of the reactor was fixed at (673 ± 5) K while *P* was set to 0.5 MPag. These operation conditions were defined previously by indication of TR.

The elemental mass balances were solved to determine the output flowrates of each component; finally, this data was used to calculate several performance indicators of the PR.

3.4. Analytical methods

3.4.1. Refractometry

This technique was chosen to verify the *S/C* ratio of the EtOH solutions used before each experiment, the equipment used is shown in Figure 11 and its manufacturing details were presented in Table 3.

First, a calibration curve was created consisting of 12 points in the range of (1 to 5) *S/C* ratio, the molar fraction of each solution was calculated considering the definition in Eq. 1 where there are 2 mol-C per 1 mol-EtOH. The solutions were prepared by mixing the corresponding volumetric fraction of synthetic EtOH and type I water measured using a micropipette. Five true replicates of each sample were analyzed in the refractometer at 298 K, the mean values of the refraction index (*RI*) were plotted, and linear regression was done (Figure 12) to obtain the calibration curve formula shown in Eq. 2. For the experiments, a tolerance limit of *S/C* ± 0.1 was determined.

$$S/C = \frac{n_{H_2O}}{2 \times n_{EtOH}} \quad \text{Eq. 1}$$

$$RI = -0.0039\,(S/C) + 1.364 \quad \text{Eq. 2}$$

Figure 11. *Refractometer RX-5000, Atago CO., LTD. Source: Author*

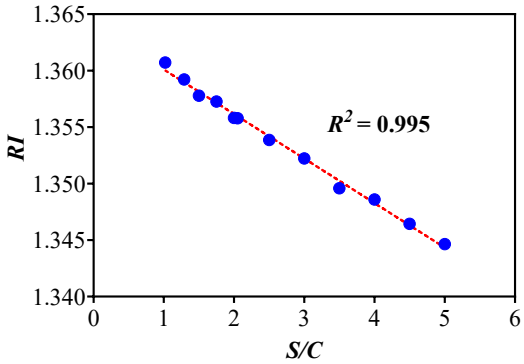

Figure 12. *Refractometer calibration curve for EtOH solutions (1 to 5) S/C ratio.*

3.4.2. Gas chromatography

This technique was used to quantify the composition of the dry gas product stream out of the PR in each experiment, the equipment used was an in-line gas chromatograph as shown in Figure 13 and its manufacturing details were presented in Table 3. This equipment has two independent columns coupled to a Thermal Conductivity Detector.

Column 1 is a CP-Molsieve 5Å that has a molecular screening coating that allows the separation of permanent gases. This column was used to quantify the following compounds in order of increasing elution time: H_2, N_2, CH_4, and CO.

Column 2 is a PoraPlot U made of a porous polymer designed to separate CO_2, C1 to C6 hydrocarbons, ketones, dissolvents, and halogenated compounds. This column was used to quantify the following compounds in order of increasing elution time: CO_2, C_2H_4, and C_2H_6.

The compounds of interest (H_2, N_2, CH_4, CO, CO_2, C_2H_4, C_2H_6) were defined by expertise and interest of the TR laboratory personnel. The operation conditions are summarized in Table 6.

Table 6*. Gas chromatography operating conditions*

Column	*T* Injector (K)	*T* Column (K)	*P* Column (MPa)	Carrier gas
CP-Molsieve 5Å	348	363	0.17	Ar gas
PoraPlot U	353	323	0.15	He gas

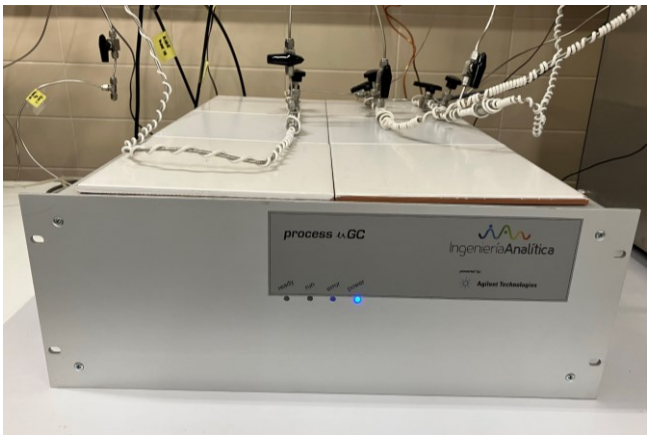

Figure 13. *Gas chromatograph process µGC, Agilent Technologies. Source: Author*

3.5. Fluid dynamics and residence time

The reactor performance could be affected by changes of mass and heat transfer phenomena associated to back mixing or channeling creating a radial gradient, thus deviating from the plug flow assumption; therefore, it was decided to check if these effects might have been significant for the PR performance [36, 37]. Based on literature, it was defined that if $H_b/Sauter\ D_c < 50$ and $D_b/Sauter\ D_c < 30$, then the transport phenomena effects might have been significant [36].

GHSV can be interpreted as the number of reactor volumes of feed at specified conditions which can be treated in unit time as calculated in Eq. 3. the linear velocity (υ_l) of the gas stream was determined using Eq. 4 as stablished in [38] considering a circular cross section. The effective velocity of the gas stream (υ_e) was determined using Eq. 5; this is a unique equation considering that it was not explicitly mentioned in any reference consulted, but rather it is a modified version proposed by the author as a result of a literature review, expecting to obtain a more accurate estimation as it incorporates advanced concepts of fluid through porous media and packed bed reactor fluid dynamics.

The basic expression between brackets of Eq. 5 was taken from [38] and modified by the tortuosity (τ) which is defined as the ratio of the channel length of the bedding and the reactor length [39], it was calculated from the experimental correlation for the tortuosity factor (τ^2) in Eq. 6 proposed by [40]. The wall effect correction factor (f_w) compensates the resistance to the flow in a bed of small diameter as consequence that the catalyst particles are packed more closely in the center of the bed but rather more disperse in the region near the wall of the container [41], it was calculated from an experimental correlation published originally by [42] as shown in Eq. 7.

Finally, the empty (t_e) and the effective (t_{er}) gas residence times were calculated using Eq. 8 and Eq. 9 respectively, as defined in [38].

$$GHSV = \frac{\dot{F}_T^{in}}{V_b} \qquad \text{Eq. 3}$$

$$\upsilon_l = 4\frac{\dot{F}_T^{in}}{\pi\, D_b^2} \qquad \text{Eq. 4}$$

$$v_e = \left(\frac{v_l}{\varepsilon}\right)\frac{\tau}{f_w} \quad \text{Eq. 5}$$

$$\tau = \sqrt{-\varepsilon\,\emptyset^{8.8788} + \left(\frac{\varepsilon}{1-\sqrt{1-\varepsilon}}\right)^{1.0534}} \quad \text{Eq. 6}$$

$$f_w = \left(1 + \frac{S_{wall}\,V_c}{2\,V_b\,A_c}\right)^2 \quad \text{Eq. 7}$$

$$t_e = \frac{H_b}{v_l} \quad \text{Eq. 8}$$

$$t_{er} = \frac{H_b}{v_e} \quad \text{Eq. 9}$$

3.6. Design of experiments

An augmented screening full factorial 2^2 + 1 center point DOE was done to evaluate the effect of *GHSV* and *S/C* on the performance of the PR before doing the initial long-run stability test. This approach was pertinent and recommended to investigate the possible interactions between variables in catalytic reactors [43] as it provided a more detailed picture of the behavior within the experimental surface that would have not been detected otherwise with a traditional One-Variable-At-Time approach [44]; additionally, it involved less unique runs than a Response Surface Methodology considering that no mathematical optimization was intended to be done for this work [45].

Five response variables were selected regarding the EtOH conversion (X_{EtOH}), the space-time yield of the main products (*STY* H_2 and *STY* CH_4), and the composition distribution as ratios of (CH_4/H_2 and CO_2/CO_x). The basic form of the equations (Eq. 10 to Eq. 14) are extensively reported in catalysis literature and were adapted for this work [46–50].

$$X_{EtOH} = \frac{\dot{N}_{EtOH}^{in} - \dot{N}_{EtOH}^{out}}{\dot{N}_{EtOH}^{in}} \times 100 \quad \text{Eq. 10}$$

$$STY\ H_2 = \frac{\dot{N}_{H_2}^{out} - \dot{N}_{H_2}^{in}}{M_{cat\,A} + M_{cat\,B}} \quad \text{Eq. 11}$$

$$STY\ CH_4 = \frac{\dot{N}_{CH_4}^{out}}{M_{cat\,A} + M_{cat\,B}} \quad \text{Eq. 12}$$

$$\frac{CO_2}{CO_x} = \frac{\dot{N}_{CO_2}^{out}}{\dot{N}_{CO}^{out} + \dot{N}_{CO_2}^{out}} \quad \text{Eq. 13}$$

$$\frac{CH_4}{H_2} = \frac{\dot{N}_{CH_4}^{out}}{\dot{N}_{H_2}^{out}} \quad \text{Eq. 14}$$

The engineering units of the independent variables were converted into coded units using Eq. 15 which is the same as replacing them by its Z-score [51], by doing this, both the model and the coded variables became orthogonal, meaning that the magnitudes of the obtained model coefficients were dimensionless making them directly comparable to determine the relative effect of the factor effects [52]. The DOE's experimental surface is shown in Figure 14, the engineering units are presented between brackets in the format of (X_1 = *GHSV*, X_2 = *S/C*), while the axis shows the corresponding coded values. Ten consecutive measures using the gas chromatograph were done after steady state was achieved. The results were

presented in standard Yate's order, notwithstanding that the experiments were conducted in random order to minimize variation errors [52].

$$X_{coded} = \frac{X_{uncoded} - \frac{X_{High} + X_{Low}}{2}}{\frac{X_{High} - X_{Low}}{2}} \quad \text{Eq. 15}$$

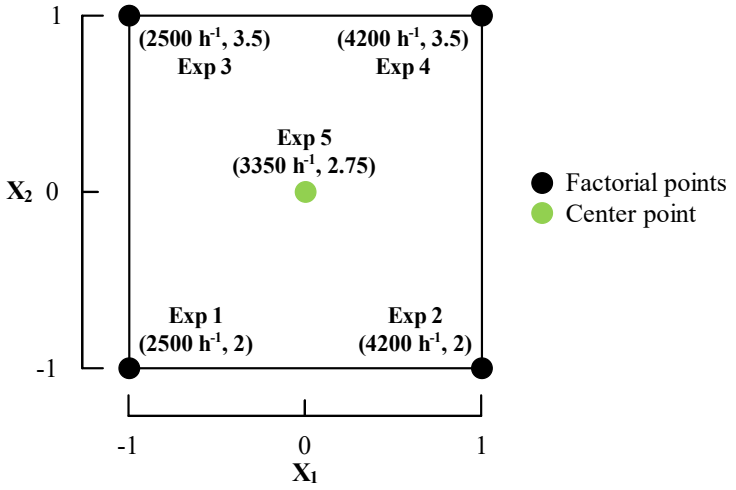

Figure 14. *Full factorial 2^2 + 1 center point DOE surface.*

To avoid misinterpretation of the results, the recommendations cited in [53] were followed to analyze the data obtained in industrial environments, the statistical significance of the factors was cautiously evaluated and assessed by determining its industrial practical significance during the decision-making process.

3.6.1. Curvature test

A full factorial 2^2 design assumes a linear response of the variables; however, there might be interactions or non-linear effects that could alter the expected flat DOE response surface. A hypothesis test can be done to detect a possible curvature of the response surface like the sum of squares for the pure quadratic curvature method proposed in [52], which only requires one degree of freedom. If the curvature is significant; then, higher-order polynomial models should be used instead of a linear model.

This test was done before the model fitting stage and it compared the average value of the responses at the factorial points with the value at the center point, the higher the difference of the means, then the non-linearity will be larger and therefore more curvature is expected as seen in Figure 15. A $\alpha = 0.05$ was chosen for a one-sample *t*-test using Statistica®, the hypotheses were stated as follows:

H0: Curvature is negligible when there is no significant difference between the average response of the factorial points compared to the center point (*p*-value > 0.05)

H1: Curvature is non-negligible when there is a significant difference between the average response of the factorial points compared to the center point (*p*-value ≤ 0.05).

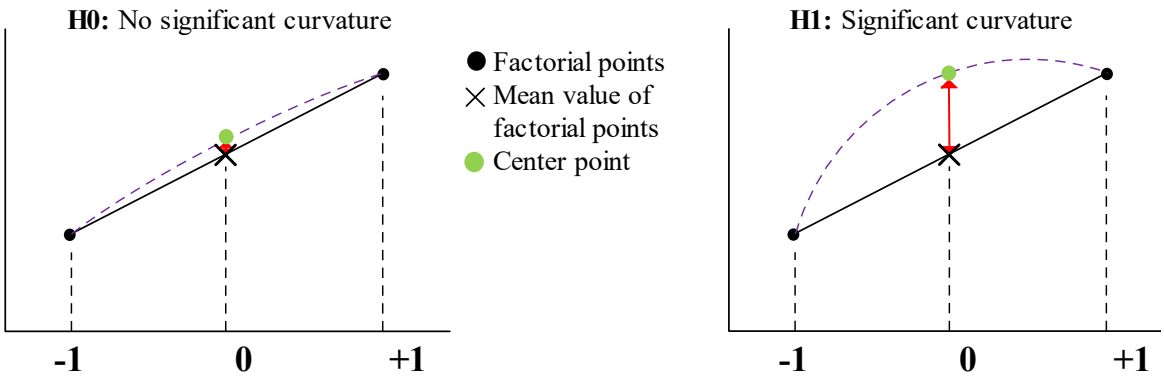

Figure 15. *Graphical representation of the curvature test.*

3.6.2. Model fitting

In this design, the center point provided one extra degree of freedom that allowed the estimation of the error even when fitting a 2-way interaction linear model [52, 53]. Then, a two-way ANOVA through Fisher's *F*-test was performed in Statistica® software to determine the effect of the independent variables on the dependent variables. With $\alpha = 0.05$, the results were considered statistically significant when *p*-value ≤ 0.05. The R^2 and R^2_{adj} were calculated to evaluate the fitness of a first order polynomial equation as shown in Eq. 16. After fitting the first model and based on the sparsity of effects principle [52], non-significant effects were pooled out to find alternative simpler models that could represent the data, interaction plots were considered for supporting the decision. 3D graphs were plotted for the final selected model.

$$\tilde{Y} = \beta_0 + \beta_1 X_1 + \beta_2 X_2 + \beta_{12} X_1 X_2 + \in \qquad \text{Eq. 16}$$

3.7. Initial long-run stability test with synthetic ethanol

Three tests were conducted to evaluate the stability of the PR at different operating conditions over time using the reactor setup already described; this three conditions were chosen by interest of TR because the results would serve them as input to perform future pilot-scale validation tests. Other process parameters remained constant. The experiment at *GHSV* 4200 h^{-1}–*S/C* 3.5 lasted for 48 h, the experiment at *GHSV* 2500 h^{-1}–*S/C* 2 lasted for 78 h, while the last experiment at *GHSV* 4200 h^{-1}–*S/C* 2 lasted for 90 h.

The results were analyzed considering the *T* and the product composition profiles; also, for each test, the same performance variables as the DOE were calculated (Eq. 10 to Eq. 14).

3.8. Selection of the best operating conditions based on the long stability results

To have an objective comparison of the results obtained with the long-run stability tests, it was necessary to transform the word "best" into a quantifiable value; to do so, a performance score indicator (PSI) was created. As seen in Eq. 17, this score balances the productivity and environmental effects, meaning that productivity KPIs were not the only values considered in the decision-making process; instead, this score is a response to the increasing demand to change the traditional chemical industry paradigm and develop more sustainable and environmentally friendly technologies [54]. The six chosen KPIs are shown in Table 7, some

of them were selected from already known green chemistry metrics considering its pertinence to this work [55].

$$PSI = \frac{\sum Score\ Productivity\ KPI}{\sum Score\ Enviroment\ KPI} \quad \text{Eq. 17}$$

***Table** 7. KPI's considered in the performance score*

Code	Category	Name	Formula	Units
KPI.1	Productivity	EtOH processing rate	$\dot{M}_{EtOH}^{in}$	g-EtOH h^{-1}
KPI.2	Productivity	Products STY	$\frac{\dot{M}_{H_2}^{out}+\dot{M}_{CH_4}^{out}}{M_{cat\ A}+M_{cat\ B}}$	g-products g-cat^{-1} h^{-1}
KPI.3	Productivity	Reaction Mass Efficiency	$\frac{\dot{M}_{H_2}^{out}+\dot{M}_{CH_4}^{out}}{\sum \dot{M}_j^{in}-\dot{M}_{N_2}^{in}}$	g-products g-reactants^{-1}
KPI.4	Environment	Process Mass intensity	$\frac{M_{cat\ A}+M_{cat\ B}+\sum \dot{M}_j^{in}}{\dot{M}_{H_2}^{out}+\dot{M}_{CH_4}^{out}}$	g-total g-products^{-1}
KPI.5	Environment	Specific Effluent generation	$\frac{\dot{M}_{Total\ Liquid}^{out}}{\dot{M}_{Total\ dry\ gas}^{out}}$	kg-effluent kg-dry_gas^{-1}
KPI.6	Environment	Specific net energy consumption	$\frac{\sum Duty^{in}-\sum Duty^{out}}{\dot{M}_{Total\ dry\ gas}^{out}}$	kJ kg-dry_gas^{-1}

KPIs were calculated considering only the initial long-run stability tests results. For each indicator, the range of the values (Max−Min) was calculated and divided into quartiles; then a score from 1 to 4 was given depending on the quartile, the higher the quartile, the higher the score. A higher score for the productivity KPIs meant higher benefits; in contrast, higher score for the environmental KPIs meant more negative impacts. A total of 12 possible points were given for productivity effects and 12 possible points for environmental impacts. The interpretation of the PSI was defined as follows:

PSI = 1 → The productivity and environmental effects were balanced.

PSI > 1 → More productivity positive effects than environmental impacts.

PSI < 1 → More environmental impacts than productivity positive effects.

The selected best conditions were later set constant to perform the exploratory reaction mechanistic study, the short-run and long-run stability test to validate the use of the PR while working with real BioEtOH.

3.9. Exploratory reaction mechanistic study

This study was done to explain the steady-state catalytic performance of the PR from a reaction mechanism point-of-view and propose a possible reaction network based on literature review. An experiment was done using EtOH at the best conditions selected from the initial long-run stability tests but loaded with just Cat A which corresponds to 60% of the reactor's loading. Gas chromatography samples were collected after the steady state was reached based on the *T* profile. It was assumed that the outlet stream from this experiment would be the input stream for the second stage of the reactor loaded with Cat B whose results were the same as the ones obtained for the corresponding experiment of the initial long-run stability test.

3.10. Short-run test using Bioethanol

Considering the best selected conditions, another experiment was done with the same experimental setup as for the DOE but using real 2nd generation BioEtOH instead of synthetic EtOH. Ten consecutive measures using the chromatograph were done after steady state was achieved based on the *T* profile. The response variables (Eq. 10 to Eq. 14) were selected to compare the performance of the PR. To determine if BioEtOH performed similar to EtOH, hypothesis tests were done in Statistica® software.

A Shapiro-Wilk test (SW) was done for each series to determine whereas the distribution may be normally distributed or not considering $\alpha = 0.05$; the test hypothesis were:

H0: If *p*-value SW > 0.05: then the null hypothesis could not be rejected, and the variable may be normally distributed.

H1: If *p*-value SW ≤ 0.05: then the null hypothesis can be rejected, and the variable is not normally distributed.

Later, a Brown-Forsythe (BF) test was done to test the assumption of homogeneity of variances considering the following hypothesis and $\alpha = 0.05$.

H0: If *p*-value BF > 0.05, then the variances are equal.

H1: If *p*-value BF ≤ 0.05, then the variances are not equal.

Finally, a student's *t*-test was performed to determine the statistical differences between the means of each grouping variable, with $\alpha = 0.05$ and considering the following hypothesis:

H0: *p*-value *t* > 0.05 , then the true difference between the group means is zero.

H1: *p*-value *t* ≤ 0.05 , then the true difference between the group means is different than zero.

3.11. Long-run test using Bioethanol

Considering the best selected conditions, a last stability test was performed using the 2nd generation BioEtOH to study the long-run performance of the PR. The test lasted for 74 h due to availability of the equipment. During the experiment, gas chromatography samples were collected at least once an hour. The equations (Eq. 10 to Eq. 14) were selected to compare the performance of the PR over time using BioEtOH against the results of the corresponding stability test done with synthetic EtOH.

During this test for BioEtOH, the *S/C* was changed from (2 to 1.5) between (7 to 23) h of reaction time, later it was set back to *S/C* 2; this was done to assess how the catalyst would respond to changes and its ability to return to its previous performance.

3.12. Aspen HYSYS® simulation

An Aspen HYSYS® simulation was used to compare the experimental results to the theoretical equilibrium conditions. Figure 16 shows the simulation equivalent to the process presented in Figure 9. A Gibbs reactor was used to determine the equilibrium compositions; T^{in}, T^{out} and *T* of the condenser were set as the ones measured experimentally. *P*-drop was considered negligible for all process equipment except pumps, 75 % adiabatic efficiency was assumed for the HPLC pump.

From literature, the recommended fluid packages for SR simulations were Soave-Redlich-Kwong, Peng-Robinson and Peng-Robinson Stryjek-Vera; preliminary simulations were done, and the results were similar with all of them as also reported in [56]; however, the Peng-Robinson Stryjek-Vera fluid package was selected as it has been used in other studies [57], also it can accurately predict H_2 phase behavior in presence of polar compounds, and it is suitable for low vapor *P* conditions [58]. This simulation was also used to estimate the theoretical net heat flow from all the heat exchangers at each process condition, this results were later used to calculate the KPI.6 to determine the best process condition.

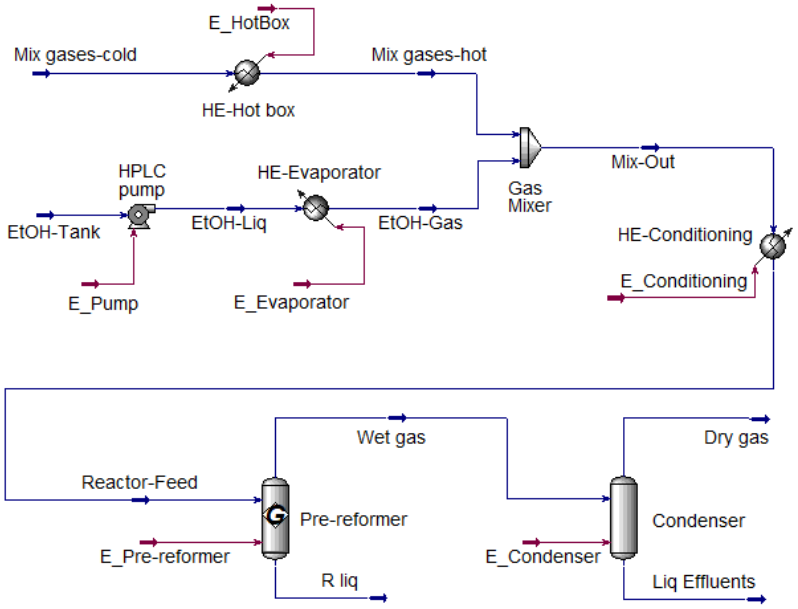

Figure 16. *EtOH pre-reforming simulation in Aspen HYSYS®.*

A summary of the activities done in this methodology and its relationship to the specific objectives can be appreciated as a flowchart in Figure 17.

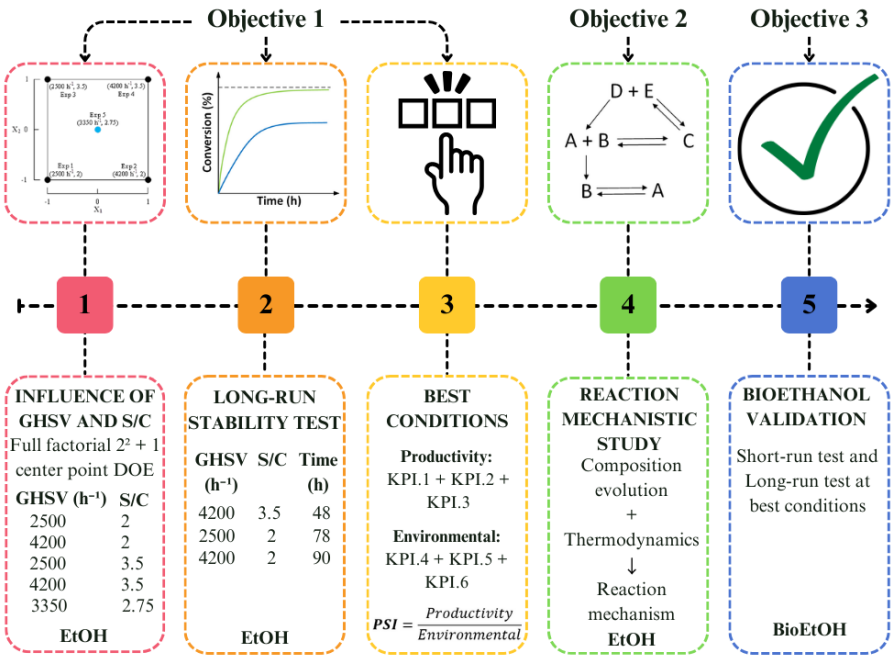

Figure 17. *Summary flowchart of the performed methodology.*

4. RESULTS AND DISCUSSION

This section exhibits the results of the methodology followed to assess the feasibility of using BioEtOH in the pre-reforming stage of a SR process to produce H_2. The results are presented in three sections related to each of the specific objectives starting from the discussion about the catalytic performance of the PR during the initial long-run stability tests at different conditions of *GHSV* (2500 to 4200) h^{-1} and *S/C* (2 to 3.5) by analyzing the product distribution, *T* profiles inside the reactor and some performance indicators like EtOH conversion and yield. Next, after deliberating about the best operating conditions, a possible reaction network is proposed to describe the performance of the PR at the best selected conditions. Finally, the results of the short-run and long-run stability tests while working with EtOH and BioEtOH are presented to compare the performance of the reactor. These results provide valuable data that can enhance the understanding of the BioEtOH pre-reforming process and to adjust its performance for the scale-up into real industrial applications.

4.1. Catalytic performance of the pre-reformer at different operating conditions

4.1.1. DOE: Influence of GHSV and S/C

Short-time real experiments were done with the PR working continuously while the conditions were changed accordingly, several gas chromatography measures were made at each state to determine the mean value of the responses that are reported in Table 8. The given values of *S/C* under the name of each experiment corresponds to the real *S/C* of the EtOH solutions measured with the refractometer, for all the experiments, the results fell within the acceptance range of *S/C* ± 0.1. The equations used for the responses were defined in the methodology (Eq. 10 to Eq. 14). C_2H_4 and C_2H_6 were detected only as traces.

***Table 8**. Calculated mean value of the DOE response variables*

Response variable	Units	Exp 1 2500 h^{-1} S/C 2.07	Exp 2 4200 h^{-1} S/C 2.07	Exp 3 2500 h^{-1} S/C 3.55	Exp 4 4200 h^{-1} S/C 3.55	Exp 5 3350 h^{-1} S/C 2.74
X_{EtOH}	%	97	95	96	99	97
$STY\ H_2$	mmol-H_2 g-cat^{-1} h^{-1}	13	31	10	23	18
$STY\ CH_4$	mmol-CH_4 g-cat^{-1} h^{-1}	26	42	16	25	25
$\frac{CO_2}{CO_x}$	mol-CO_2 mol-CO_x^{-1}	0.94	0.91	0.94	0.94	0.94
$\frac{CH_4}{H_2}$	mol-CH_4 mol-H_2^{-1}	2.09	1.34	1.64	1.08	1.39

4.1.1.1. Curvature test

The statistical analysis of the DOE started with the curvature test for each response variable as seen in Table 9. For all response variables, the *p*-value *t* was > 0.05; therefore, there was not enough evidence to reject the null hypothesis resulting in a high probability that the response surface of the DOE space within the given limits might have had no significant curvature for all the calculated response variables [59]. Additionally, it was concluded that a linear model as the one presented in Eq. 16 could be adequate to display the response of the variables within the experimental space and no quadratic effects were expected [52].

***Table 9**. Curvature test results for the full factorial 2^2+center point DOE*

Response variable	Units	Factorial points mean	Factorial points SD	Center point value	*t*-value	*p*-value
X_{EtOH}	%	97	2	97	-0.1	0.9
$STY\ H_2$	mmol-H_2 g-cat^{-1} h^{-1}	19	10	18	0.3	0.8
$STY\ CH_4$	mmol-CH_4 g-cat^{-1} h^{-1}	27	11	25	0.5	0.7
$\frac{CO_2}{CO_x}$	mol-CO_2 mol-CO_x^{-1}	0.93	0.02	0.94	-0.8	0.5
$\frac{CH_4}{H_2}$	mol-CH_4 mol-H_2^{-1}	1.54	0.43	1.39	0.7	0.5
S_P	Mol-prod mol-total^{-1}	0.765	0.006	0.766	-0.3	0.8

4.1.1.2. Performance based on EtOH *conversion*

Conversion is the most basic yet most important parameter to appraise the performance of a catalytic reactor. The interaction plot in Figure 18 suggested that the main effects of the coded variables X_1 (*GHSV*) and X_2 (*S/C*) over the response X_{EtOH} might not have been significant while the strong interaction among them could explain the results within the DOE surface. Later, the ANOVA results in Table 10 confirmed that only the interaction term X_1X_2 was significant for the model options 1 and 2. Between them, option 1 was chosen because it contained a significant effect whilst the two main effects were close to becoming significant. R^2 and R^2_{adj}showed good fit. Figure 19 shows the 3D response of the variable as a shape of folded sheet due to the interaction term. As proven, the conversion of the PR was the result of the mutual interaction of *GHSV* and *S/C* leading to different results in the experiments.

***Table 10**. ANOVA analysis of models to study the effect of GHSV and S/C on EtOH conversion*

Option	Model type	R^2	R^2_{adj}	*p*-value X_1	*p*-value X_2	*p*-value X_1X_2	Error MS
1	2-way inter	99.9	99.4	0.10	0.06	0.03[a]	0.01
2	2-way inter	93.6	87.0	n/c[b]	0.14	0.04[a]	0.23
3	2-way inter	81.5	63.1	0.49	n/c[b]	0.10	0.66
4	2-way inter	75.2	66.9	n/c[b]	n/c[b]	0.06	0.59
5	No inter	24.7	0.0	0.72	0.56	n/c[b]	2.69

[a] Statistically significant at *p*-value ≤ 0.05
[b] Not considered in the model

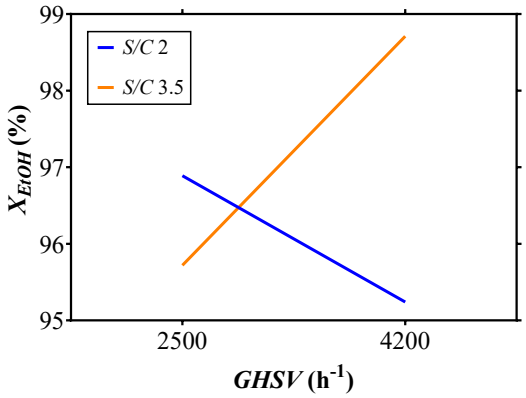

***Figure 18.** Interaction plot for EtOH conversion*

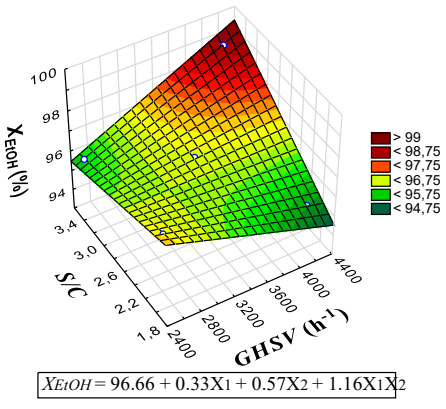

***Figure 19.** Response surface for EtOH conversion*

Based on literature, these results seems acceptable since depending on the conditions, different conversions can be achieved and conversion values of 100% are not rare. For example, X_{EtOH}>90% was obtained using a Co/SiO_2 catalyst at 673 K, *S/C* 1.5, 2 cm^3 h^{-1}; and X_{EtOH}>85% was obtained using a NiNPs/OH-MBeta catalyst [17]. Acknowledging that all the results were greater than 90% for this response in the DOE and from an industrial perspective, this difference among them was not considered relevant as the tested conditions provided acceptable performance based on the conversion.

4.1.1.3. Performance based on H_2 yield

The catalytic activity of the reactor towards H_2 was assessed through this response variable which represents how much H_2 was generated over the PR loading. The interaction plot in Figure 20 suggested that the main effects of *GHSV* and *S/C* might be significant while the interaction term was not. That observation was later confirmed through the ANOVA results of each proposed model in Table 11 where the *GHSV* term X_1 was significant for model options 1 and 5. Model 5 was selected to represent the behavior of the response as it was proven that interaction term was not relevant and the difference between the regression coefficients showed a good balance explaining the variance of the responses. Figure 21 shows the 3D response of the variable as a highly linear sheet without interactions.

***Table 11**. ANOVA analysis of models to study the effect of GHSV and S/C on STY H_2*

Option	Model type	R^2	R^2_{adj}	*p*-value X_1	*p*-value X_2	*p*-value X_1X_2	Error MS
1	2-way inter	99.5	97.9	0.05[a]	0.14	0.3	1.5
2	2-way inter	12.5	0.0	n/c[b]	0.68	0.8	126.7
3	2-way inter	89.6	79.1	0.06	n/c[b]	0.6	15.1
4	2-way inter	2.6	0.0	n/c[b]	n/c[b]	0.8	94.0
5	No inter	96.9	93.9	0.02[a]	0.13	n/c[b]	4.4

[a] Statistically significant at *p*-value ≤ 0.05

[b] Not considered in the model

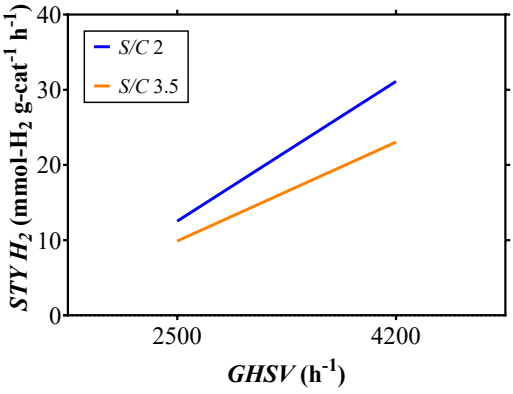

***Figure 20.** Interaction plot for STY H_2*

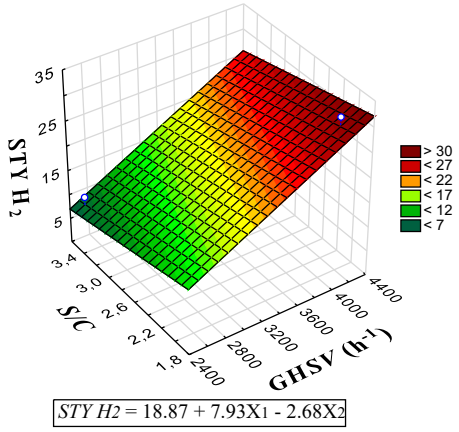

***Figure 21.** Response surface for STY H_2*

It was concluded that the increase of the H_2 productivity was significant because of *GHSV*, where higher values represented more yield. Physically it makes sense considering also the observations made for the conversion in the previous section; if greater inlet gas flowrate can be treated without a significant reduction of the conversion, then a higher H_2 throughput

is expected. The graphs also evidenced that higher H_2 yield was observed at the lower limit of *S/C*, although this effect was not statistically significant with *p*-value>0.05 for model 5.

Especially for catalytic processes, a direct comparison of these results to other studies is not possible since many factors can affect the performance of a catalyst. For example, the study conducted by [60] obtained 45 mmol-H_2 g-cat^{-1} h^{-1} using a CaZr-Ni catalyst at 673 K, *GHSV* of 2700 h^{-1} and steam to EtOH ratio 3; however, at the same conditions and same composition of catalyst but prepared with another method resulted in a productivity of 18 mmol-H_2 g-cat^{-1} h^{-1}. Thus, for this variable it was enough just to recognize that the obtained *STY* H_2 values in the present work were within similar reported ranges; additionally, it was concluded that lower values of *S/C* and higher values of *GHSV* can be related to higher H_2 productivity yield.

4.1.1.4. Performance based on CH_4 yield

The analysis of the yield values for CH_4 proceeded similarly as for H_2. The interaction plot of Figure 22 suggested a possible effect of both main factors without an interaction term. From the ANOVA results depicted in Table 12, model 5 was selected as it included the statistically significant effect of X_2; it should be noticed that the X_1 effect was close to be significant, meaning that for a real application it should not be discarded for the same reason as it was demonstrated for the H_2 yield. As seen in Figure 23, lower values of *S/C* and higher values of *GHSV* can be related to higher CH_4 productivity yield.

***Table 12**. ANOVA analysis of models to study the effect of GHSV and S/C on STY CH_4*

Option	Model type	R^2	R^2_{adj}	*p*-value X_1	*p*-value X_2	*p*-value X_1X_2	Error MS
1	2-way inter	98.5	93.8	0.12	0.11	0.37	5.4
2	2-way inter	56.2	12.5	n/c[b]	0.26	0.72	76.0
3	2-way inter	45.9	0.0	0.34	n/c[b]	0.75	93.9
4	2-way inter	3.7	0.0	n/c[b]	n/c[b]	0.76	111.5
5	No inter	94.8	89.5	0.06	0.05[a]	n/c[b]	9.1

[a] Statistically significant at *p*-value ≤ 0.05

[b] Not considered in the model

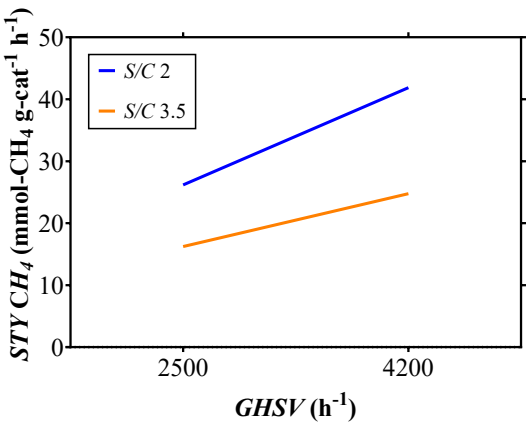

***Figure 22.** Interaction plot for STY CH_4*

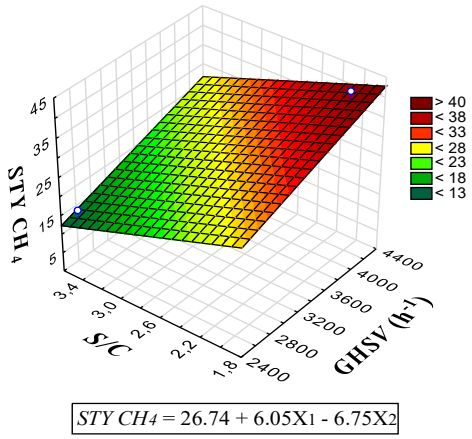

$STY\ CH_4 = 26.74 + 6.05X_1 - 6.75X_2$

***Figure 23.** Response surface for STY CH_4*

4.1.1.5. Performance based on CO_2/CO_x ratio

The interaction plot in Figure 24 showed a possible dominant interaction effect, although the closeness of the lines suggested no significant effects at all. A detailed review of the individual mean values reported in Table 8 showed that only the response for Exp 2 differed from the others by 3% which is a small difference that can be associated to some experimental deviation during that test; therefore, neither of the main or interaction effects might have been relevant to explain this response variable. The observation was also proven by the results of the ANOVA analysis in Table 13 where neither of the proposed models showed a statistically significant effect of *GHSV* and *S/C* over the distribution of CO and CO_2. Since no appreciable effect was confirmed, instead of fitting a model without any significant effects, it was decided to prove this behavior from a theoretical point of view.

Figure 25 shows the product distribution graph from a thermodynamic study conducted by [61], no significant variations were identified for the CO_2/CO_x even when changing the *S/C* at *T* below 673 K. With an average experimental value of 0.94 for the CO_2/CO_x ratio and remembering that 673 K was the working *T* of the experimental PR, the DOE results matched the expected value based on the thermodynamic calculations from the reference study. Thus, confirming that the PR performed as expected at any working conditions of *GHSV* and *S/C* showing that CO and CO_2 had no significant change.

***Table 13**. ANOVA analysis of models to study the effect of GHSV and S/C on CO_2/CO_x ratio*

Option	Model type	R^2	R^2_{adj}	*p*-value X_1	*p*-value X_2	*p*-value X_1X_2	Error MS
1	2-way inter	95.8	83.4	0.2	0.2	0.3	3×10^{-5}
2	2-way inter	62.4	24.8	n/c[a]	0.3	0.4	2×10^{-4}
3	2-way inter	50.9	1.7	0.4	n/c[a]	0.5	2×10^{-4}
4	2-way inter	17.4	0.0	n/c[a]	n/c[a]	0.5	2×10^{-4}
5	No inter	78.4	56.8	0.2	0.2	n/c[a]	9×10^{-5}

[a] Not considered in the model

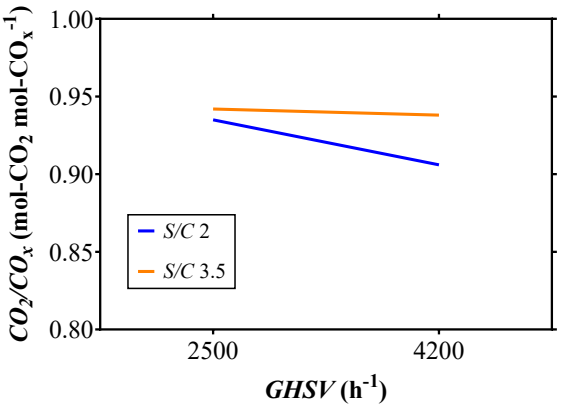

***Figure 24.** Interaction plot for CO_2/CO_x ratio*

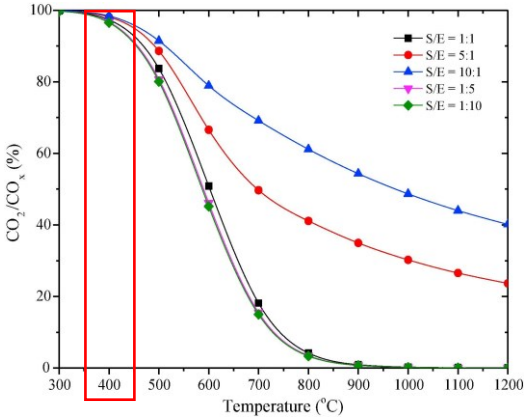

***Figure 25.** Thermodynamic CO_2/CO_x distribution at different S/C. Source:* [61]

4.1.1.6. Performance based on CH_4/H_2 ratio

Considering the previously discussed experimental results, C_2H_4 and C_2H_6 were not relevant for the product distribution, also the CO_2/CO_x ratio remained inalterable at steady-state conditions; hence, the CH_4/H_2 ratio was the most influential to describe the performance of the PR and product distribution. The interaction plot in Figure 26 suggested no significant interaction effects among the independent and the dependent variables, whilst the main effects of *GHSV* and *S/C* might had been significant. The summary of the ANOVA analysis in Table 14 indicated that the X_1 effect corresponding to *GHSV* was statistically significant to model the distribution while the X_2 effect of *S/C* had a minor impact. The model option 5 was used to plot Figure 27. It was proven that CH_4/H_2 ratio decreased at higher *GHSV* values, this shows accordance to the previously discussed *STY* results where higher values of *GHSV* increase the yield of H_2 while lowering the yield of CH_4; thus, explaining why the ratio decreased.

***Table 14**. ANOVA analysis of models to study the effect of GHSV and S/C on CH_4/H_2 ratio*

Option	Model type	R^2	R^2_{adj}	*p*-value X_1	*p*-value X_2	*p*-value X_1X_2	Error MS
1	2-way inter	96.9	87.6	0.13	0.23	0.63	0.02
2	2-way inter	23.3	0.0	n/c[b]	0.53	0.87	0.22
3	2-way inter	74.9	49.9	0.14	n/c[b]	0.78	0.07
4	2-way inter	1.3	0.0	n/c[b]	n/c[b]	0.85	0.19
5	No inter	95.6	91.1	0.03[a]	0.09	n/c[b]	0.01

[a] Statistically significant at *p*-value ≤ 0.05

[b] Not considered in the model

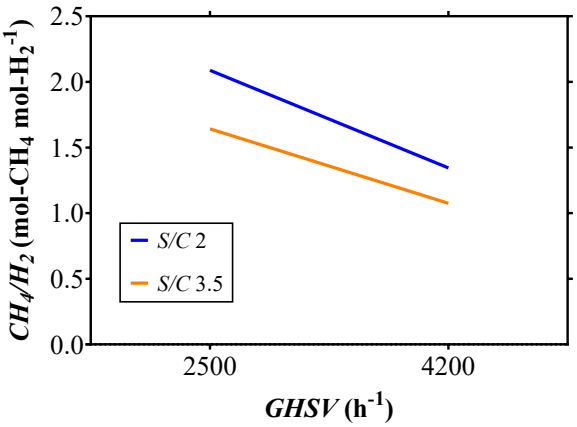

***Figure 26.** Interaction plot for CH_4/H_2 ratio*

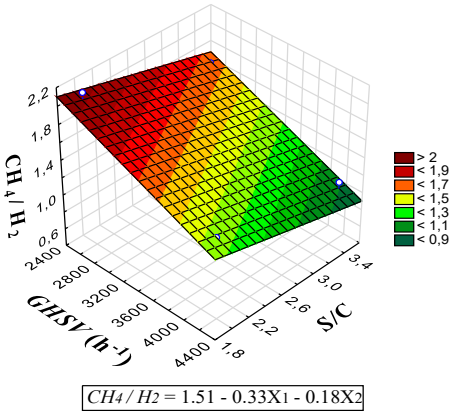

***Figure 27.** Response surface for CH_4/H_2 ratio*

4.1.2. Initial long run stability tests

Three tests were conducted to evaluate the stability of the PR at different operating conditions over time based on the interest of TR to perform future pilot-scale validations (*GHSV* 4200 h^{-1}–*S/C* 3.5, *GHSV* 2500 h^{-1}–*S/C* 2, and *GHSV* 4200 h^{-1}–*S/C* 2).

4.1.2.1. Composition distribution profile

To start the analysis of the stability tests, Table 15 shows the results for the fluid dynamics parameters. *GHSV* ultimately defined the working flowrates of the experiments as shown in Eq. 3; whereas *S/C* defined the composition of the inlet stream; thus, the residence time was

independent of *S/C*. According to theory, the velocity of a fluid through a porous media like a packed bed reactor must be faster than the velocity in a void vessel like an empty plug flow reactor in order to preserve its momentum [38]; in this sense, the results agreed with the theory showing that the calculated values of v_e were greater than the values of v_l for the tested *GHSV* values. Accordingly, if a fluid flows faster, it is expected to have less residence time inside the reactor [38]; this was also demonstrated mathematically by obtaining lower values of t_{er} compared to the ones for t_e. Thus, it was proven that increasing *GHSV* undoubtedly resulted in less residence time inside the reactor for the reactions to take place. Understanding these interdependencies were crucial for a better understanding and explanation of the continuous flow operation results in the following sections [47].

***Table 15**. Pre-reformer fluid dynamics parameters depending on GHSV*

GHSV **(h^{-1})**	***S/C***	v_l **(m s^{-1})**	v_e **(m s^{-1})**	t_e **(ms)**	t_{er} **(ms)**
2500	2	0.03	0.10	1440	502
4200	2	0.06	0.17	857	300
4200	3.5	0.06	0.17	857	300

The composition distribution in the long-run stability tests are presented in Figure 28 (Next page). At first glance, the profiles showed that surely the combination of *S/C* and *GHSV* had an effect on the performance of the PR, especially for the distribution of the main products where H_2 varied in the range of (25 to 35)% whereas CH_4 did between (32 to 44)%; CO and CO_2 did not vary considerably and remained around the 19% and 0.8% composition respectively; Finally, in all three experiments, the intermediate products C_2H_4 and C_2H_6 were detected only as traces under 0.02% composition. In general, the product distribution followed the tendency predicted by the Gibbs reactor in the HYSYS® simulation represented by discontinuous lines in the graphs, CH_4 was dominant at the lower value of *S/C* experiments while H_2 was dominant in the experiment at the higher value of *S/C* 3.5.

There are diverse reasons to justify the small deviation of the measured compositions compared to the equilibrium results; for example, the protocol used for the loading of the catalyst might had an impact; this based on reports in literature about stagnation and hotspot zones that could have altered the residence time and affected the process efficiency due to improper packing [47]. Also, considering the measured $Sauter\ D_c$, it was determined that $H_b/Sauter\ D_c < 17$ and $D_b/Sauter\ D_c < 6$, based on the definition set in the methodology, this supported the hypothesis that other phenomenon related to mass and heat transfer effects might have happened altogether slightly affecting the performance; nevertheless, it was concluded that the reactor performed accordingly converting EtOH into the expected products near the theoretic thermodynamic equilibrium.

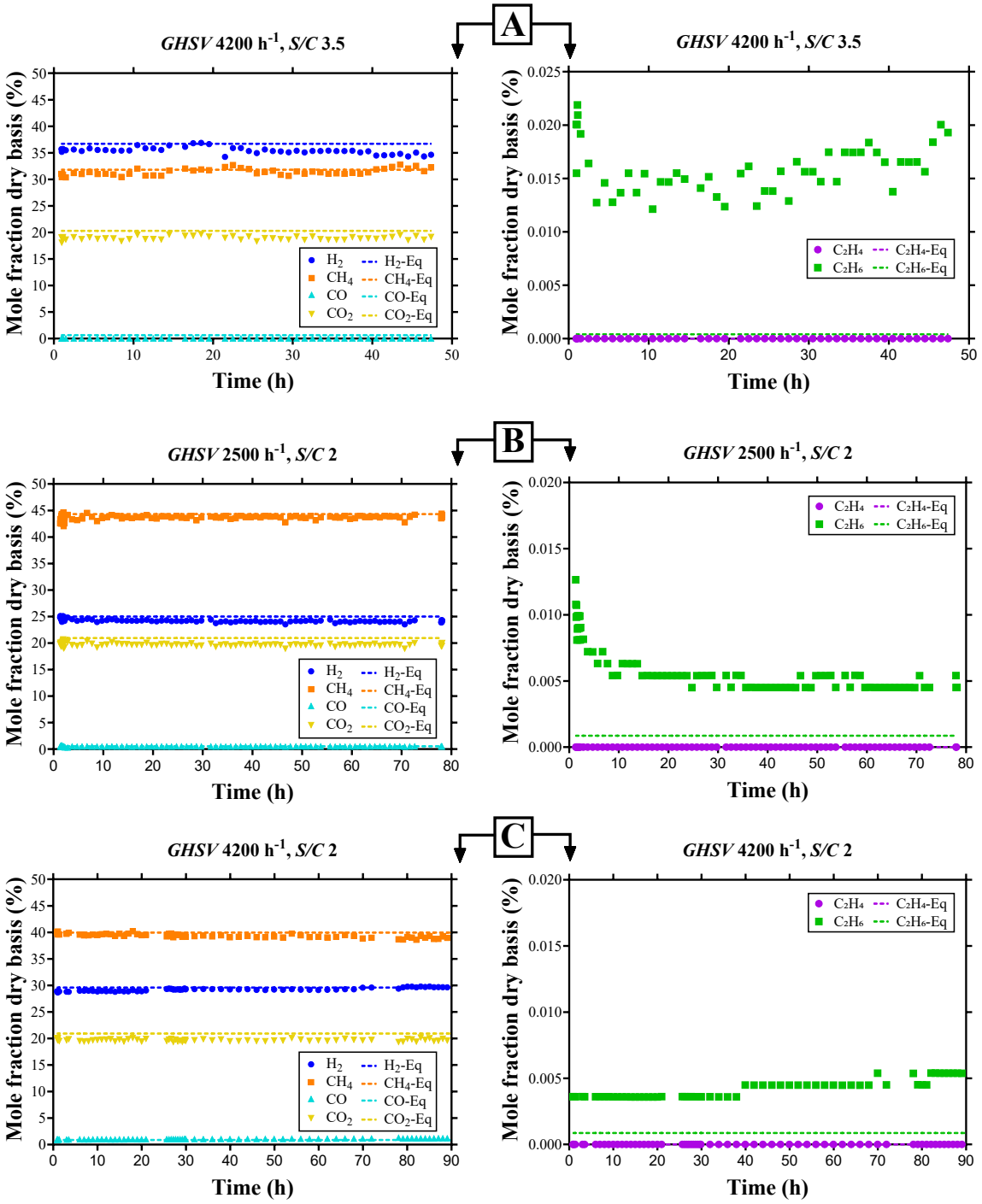

Figure 28. *Output gas product distribution of the long-run stability tests at 673 K, 0.5 MPag* ***A)*** *4200 h^{-1} - S/C 3.5,* ***B)*** *2500 h^{-1} - S/C 2,* ***C)*** *4200 h^{-1} - S/C 2*

The experiment at 4200 h^{-1}–*S/C* 3.5 had more selectivity towards H_2 compared to the other experiments. In this case, the combination of *S/C* and *GHSV* might had shifted the catalytic reaction pathways towards one or other product explaining the result obtained which was also consistent with the simulation. This behavior can also be explained from a thermodynamic point of view.

Figure 29 shows the results of a study case in HYSYS® where the product distribution changed depending on the *T* and the *S/C*; it is seen that the inversion between the dominancy

of CH_4 towards H_2 is plausible an depends on the *S/C*. Lower *S/C* has an inversion point at higher *T*, while higher values of *S/C* have the inversion at lower *T*. Since T^{in} was constant at 673 K for all the experiments, then the product distribution could be attributed mainly to the *S/C* ratio; for example, the 4200 h^{-1}–*S/C* 3.5 was operating in the H_2 dominant region, while the 4200 h^{-1}–*S/C* 2 was working in the CH_4 dominant part of the distribution.

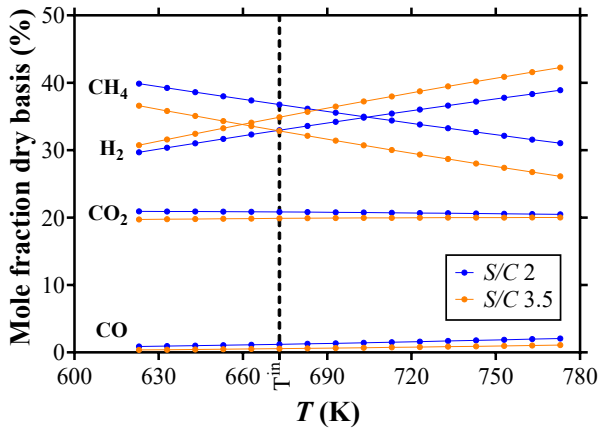

Figure 29. *EtOH pre-reforming product distribution as a function of T and S/C. Source: Author*

4.1.2.2. Temperature profile

The *T* profile in each experiment was monitored continuously at eight points along the reactor, the mean values over time are presented in Figure 30. All three experiments had the same profile characterized by a steep descent of *T* until about 50% of the reactor loading, the second half of the reactor showed higher *T* compared to the inlet.

As mentioned in the literature chapter, EtOH catalytic pre-reforming is achieved through a complex reaction network; depending on the process conditions and the catalysts used, some reactions pathways become more dominant than others. In this sense, considering the two-stage reactor configuration used for this experiments, Cat A would promote predominantly endothermic reactions like EtOH dehydrogenation and dehydration while Cat B would promote mostly exothermic reactions of the products obtained after the first section of the reactor like methanation and water-gas shift giving out an overall exothermic profile characterized by higher T^{out} compared to T^{in}. This endothermic/exothermic *T* profile has been reported in literature for PRs [62]. A detailed explanation of this phenomenon will also be discussed in a later section of this report from a reaction mechanics point of view.

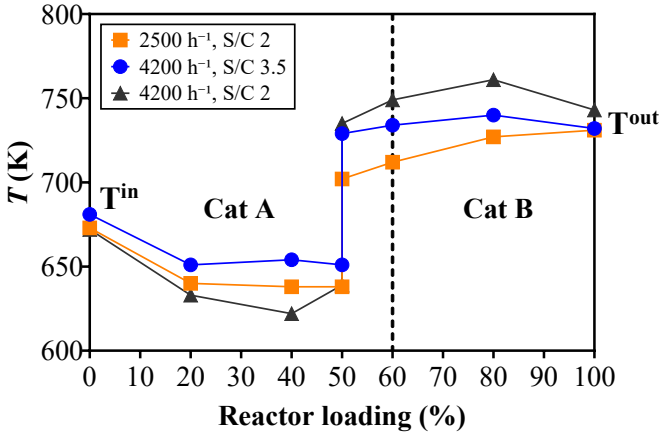

Figure 30. *T profiles along the PR for the EtOH initial long-run stability test*

The notorious increase of the T at the 50% reactor loading could be related to the proximity of that zone of the reactor to the heating resistance of the furnace but also influenced by the exothermic behavior of the reactions occurring in the Cat B section.

The *T* profiles also suggested a possible influence of *GHSV* and *S/C*. The experiments at *S/C* 2 had a steeper descent compared to *S/C* 3.5, meaning that more endothermic reactions were occurring possibly due to higher concentration of EtOH that was being pre-reformed to gaseous products. Similarly, the *T* profile in the exothermic region was higher for the experiment 4200 h^{-1}–*S/C* 2 possibly related to more gaseous compounds being transformed via exothermic pathways like the methanation and water-gas shift reactions.

Finally, the experiments at the same *S/C* 2 but different *GHSV* showed a difference in the *T* profiles, the *T* descent at 2500 h^{-1} was less pronounced compared to the experiment at 4200 h^{-1}, the answer could be related to the flowrate where higher flowrates represents more EtOH per unit of time, increasing the total amount at the inlet and resulting in more feedstock to be pre-reformed.

In conclusion, the forementioned first observations based on the composition and *T* profiles confirmed a relationship between the pre-reforming operating parameters and the performance of the reactor in the long-run steady-state conditions.

4.1.2.3. Performance based on conversion, yield and composition distribution

The response variables used for the DOE were also calculated for the initial long-run stability tests to identify their evolution over time. Figure 31 shows the EtOH conversion where all experiments displayed good stability with no major changes over 90% conversion; these results agreed to the ones obtained in the DOE showing that the catalysts were not significantly affected during the run time.

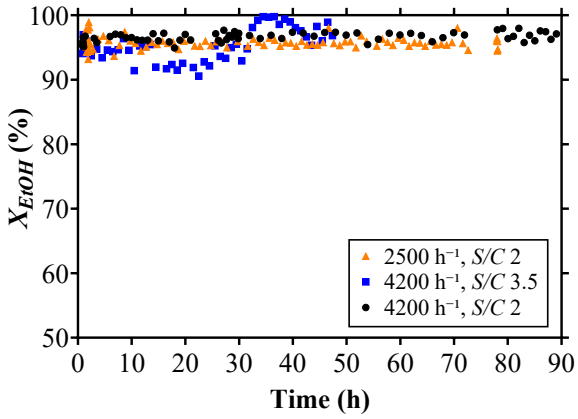

Figure 31. *Evolution of EtOH conversion over time for the long-run stability tests at 673 K, 0.5 MPag*

Regarding the *STY* H_2, the highest value was achieved by 4200 h^{-1}–*S/C* 2, followed closely by 4200 h^{-1}–*S/C* 3.5; below them, 2500 h^{-1}–*S/C* 2 produced 56% less compared to the highest value. This results matched exactly the behavior described in the DOE (Figure 20) and confirmed that H_2 yield was influenced mostly by *GHSV* rather than *S/C* as seen in Figure 32. H_2 productivity was stable over time; no significant changes were detected except for the experiment at *GHSV* 4200 h^{-1}–*S/C* 3.5 which *STY* was stable until 20 h and later dropped by 9% at 48 h time when it was decided to stop the experiment. This drop was due to the start of coke formation that was identified after opening the PR.

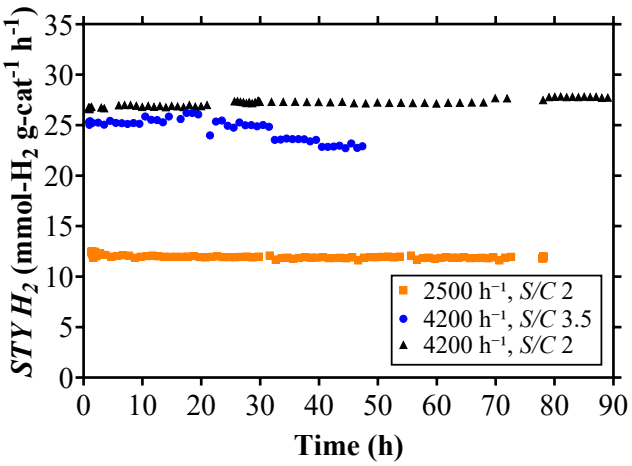

Figure 32. *Evolution of STY H_2 over time for the long-run stability tests at 673 K, 0.5 MPag*

In a similar way, Figure 33 shows the response of *STY CH_4*, it followed the same behavior as described in the DOE where the highest value was achieved by 4200 h^{-1}–*S/C* 2, followed by 4200 h^{-1}–*S/C* 3.5 and 2500 h^{-1}–*S/C* 2 (Figure 21) with similar value between the last two. CH_4 production was stable during the test.

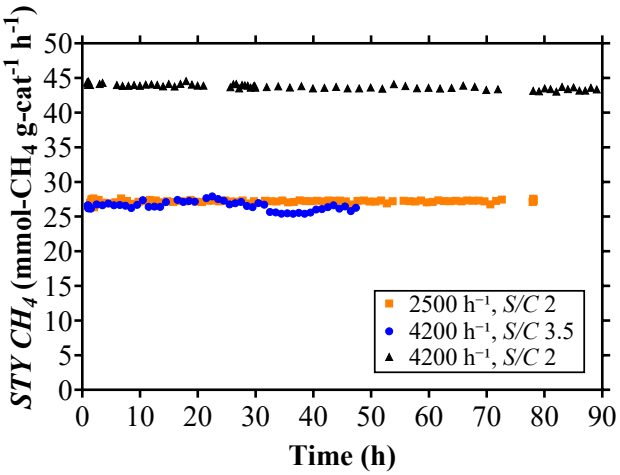

Figure 33. *Evolution of STY CH_4 conversion over time for the long-run stability tests at 673 K, 0.5 MPag*

Moving to the *CO_2/CO_x* ratio, the results of the long-run stability test showed no significant change for CO and CO_2 over time and remained stable in values over 0.94 as predicted thermodynamically (Figure 34) and matching the same behavior as described in the DOE. Thus, confirming that *GHSV* and *S/C* had no influence over this response variable.

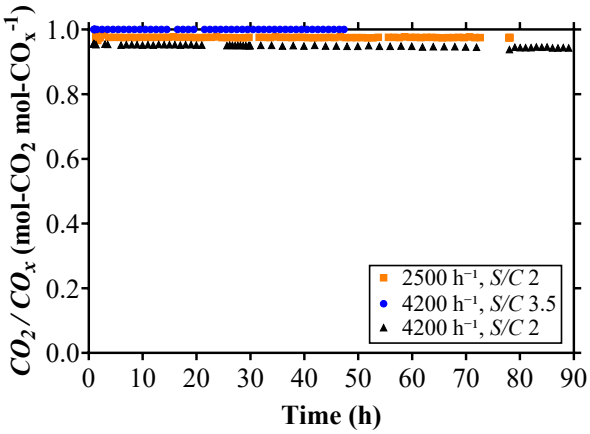

Figure 34. *Evolution of CO_2/CO_x over time for the long-run stability tests at 673 K, 0.5 MPag*

Finally, the results of the long-run stability tests matched exactly the predicted behavior with the DOE, the lowest value of CH_4/H_2 ratio was obtained by experiment at 4200 h^{-1}–*S/C* 3.5, whereas the highest value was obtained at 2500 h^{-1}–*S/C* 2, this can be seen by comparing the results in Figure 26 and Figure 35. The ratio of these compounds was stable for all three experiments, demonstrating an outstanding performance of the PR at the tested conditions under steady-state. Also, it was concluded that the PR product distribution followed the expected theoretical tendency and explained the notorious change of CH_4 and H_2 distribution in the composition graphs as it was discussed for the DOE study. Also, as it was discussed for Figure 29, *S/C* could shift the selectivity towards H_2 production depending on thermodynamic favorability without altering the conversion.

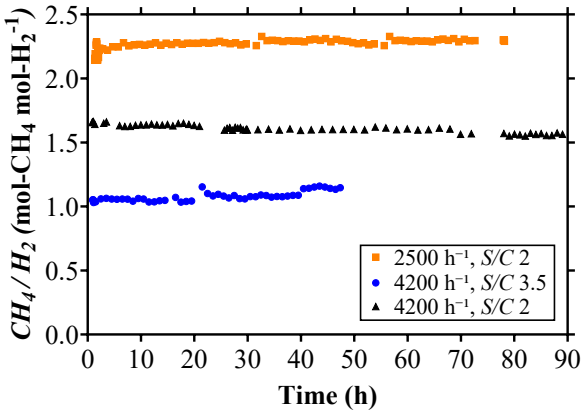

Figure 35. *Evolution of CH_4/H_2 over time for the long-run stability tests at 673 K, 0.5 MPag*

Some concluding remarks about the catalytic performance of the PR at different operating conditions considering the DOE results and the confirmation of their behavior during long-run stability tests:

- The obtained EtOH conversion values for all experiments were in the range of (95 to 99)%; from an industrial perspective, this meant that all process conditions were suitable for a potential scale-up process since no significant differences were determined among them.
- Lower values of *S/C* and higher values of *GHSV* could be related to higher H_2 and CH_4 yield; significant differences were determined among the experiments. Thus, this

productivity parameters could be industrially relevant to select a possible best operating scenario.

- The average value of CO_2/CO_x ratio remained constat around 0.94 for all the experiments, perfectly matching the thermodynamic predictions. Thus, this parameter was not considered relevant to select a possible best operating scenario.
- The average value of CH_4/H_2 varied significantly along the experimental space, an inverse relationship between the compositions of these compounds was detected. If the H_2 fraction increased, undoubtedly the CH_4 fraction would decrease and vice-versa. Lower ratios were obtained at high *GHSV* values; also, lower ratios were determined at higher values of *S/C*. Considering that the output stream of this PR will be later the input of the main steam reformer where the carbon oxides would be converted into H_2, then, the product distribution is not adequate to carefully select a possible best operating scenario. **It is worth mentioning that higher values of CH_4 compared to H_2 are accepted because the goal of the pre-reformer is to convert EtOH into lighter compounds but not necessarily maximizing the H_2 production.**
- Coke was not detected in any of the experiments, indicating that the catalysts were not significantly poisoned and explaining the stable performance over time in all calculated variables.

4.1.3. Selection of the best operating conditions

The selection of the best operating conditions considered TR's interest to possibly work at the studied conditions of the long-run stability test in a later pilot scale test using real BioEtOH; thus, the selection needed to be thoughtful to justify the best case condition. Considering the results of the initial long-run stability tests, the KPIs described in Table 7 were calculated which results are shown in Table 16, they served as input for the scoring procedure described in the methodology resulting in the score chart presented in Figure 36.

***Table 16**. Calculated KPI values to select the best operating conditions based on stability tests*

Code	Name	Units	4200 h^{-1} *S/C* 3.5	2500 h^{-1} *S/C* 2	4200 h^{-1} *S/C* 2
KPI.1	EtOH processing rate	g-EtOH h^{-1}	12.6	12.0	20.2
KPI.2	Products *STY*	g-products g-cat^{-1} h^{-1}	0.5	0.5	0.8
KPI.3	Reaction Mass Efficiency	g-products g-reactants^{-1}	13.8	20.6	20.0
KPI.4	Process Mass intensity	g-total g-products^{-1}	131.3	133.8	83.5
KPI.5	Specific Effluent generation	kg-effluent kg-dry gas^{-1}	1.5	1.0	0.9
KPI.6	Specific net energy consumption	kJ kg-dry gas^{-1}	356.0	50.8	267.8

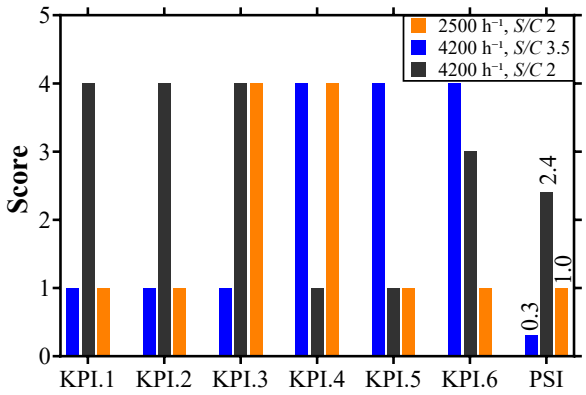

***Figure 36.** PSI score given to each evaluated condition based on the KPI values*

The experiment working at 4200 h^{-1}–*S/C* 3.5 was directly discarded because its PSI score was lower than 1, meaning that those process conditions would have more environmental impacts than actual productivity benefits. The experiment at 2500 h^{-1}–*S/C* 2 had a balanced result with PSI = 1, whilst the experiment at 4200 h^{-1}–*S/C* 2 had more positive productivity effects than environmental impacts with PSI = 2.4. A closer look to the individual KPI's scores supported the evidence:

KPI.1 showed that the experiment at 4200 h^{-1}–*S/C* 2 provided 60% more EtOH processing rate compared to the second-best option, which is desired from an industrial perspective by allowing more production capacity.

KPI.2 showed that the experiment at 4200 h^{-1}–*S/C* 2 would generate the highest production rate of H_2 and CH_4 among the other options with a throughput 40% higher compared to the second-best option.

KPI.3 showed that the experiment at 4200 h^{-1}–*S/C* 2 would convert around 20% of the raw materials into the desired products.

KPI.4 considered the total mass needed to obtain the products, including reactants, inert gases, and catalysts. Lower values were appreciated meaning that less mass is required to obtain a unit of mass of products. The experiment at 4200 h^{-1}–*S/C* 2 had the lowest impact in this parameter.

KPI.5 compared the liquid effluent generated in the condenser, lower values were appreciated since it would represent less volume to be treated or recycled back to the process. Among the options, the experiment at 4200 h^{-1}–*S/C* 2 had the lowest value.

KPI.6 assessed the net energy requirement to obtain 1 kg of dry gas. In this case the best option was the experiment at 2500 h^{-1}–*S/C* 2 since it had the lowest value, while the experiment at 4200 h^{-1}–*S/C* 2 was the second option. However, it was important to consider that the experiment at 4200 h^{-1}–*S/C* operated at higher *GHSV* than experiment at 2500 h^{-1}–*S/C* 2. Thus, the additional energy required was result of the increased demand of flowrate as confirmed in [63]. Although more energy was required, the productivity KPI balanced the energy consumption. Finally, it should be noticed that this result comes from the simulation without energy integration or recovery; thus, less energy demand should be expected for the industrial application after considering this operating scenario.

Based on the PSI score and the detailed analysis of each KPI, the experiment at 4200 h^{-1}–*S/C* 2 was selected as the best operating condition considering the interest to select a highly productive process, with the lowest steam intensity and the least environmental impacts. Despite the fact that this configuration would enhance more CH_4 than H_2 production, it was accepted considering that the goal of the PR is to convert EtOH into lighter compounds which later will be treated I the main steam reforming stage. These parameters were established to perform the exploratory reaction mechanistic study, the short-run, and long-run stability tests to validate the possible use of BioEtOH at the selected PR configuration.

4.2. Exploratory reaction mechanistic study

The advanced understanding of the reaction mechanism is an essential step to improve a catalytic process [64]. Hence, an exploratory mechanistic study was performed to understand the evolution of the species along the PR at the best selected conditions from the stability tests (4200 h^{-1}, *S/C* 2) using EtOH. Figure 37 shows the average composition of each compound measured experimentally at three points along the reactor, the inlet at 0% loading, the outlet after Cat A section at 60% loading, and the outlet after Cat B section at 100%

loading that is the output stream of the PR. The composition at the outlet of Cat A was determined through an experiment using the same conditions of *GHSV* 4200 h^{-1} and *S/C* 2 but without the Cat B section; the compositions at the outlet of Cat B section were the same as the ones determined during the initial long-run stability test for EtOH; the composition of the inlet was common for both experiments, water and N_2 were not considered for the plot but were used in the experiments, the dotted lines represent the expected values at thermodynamic equilibrium calculated with the HYSYS® simulation.

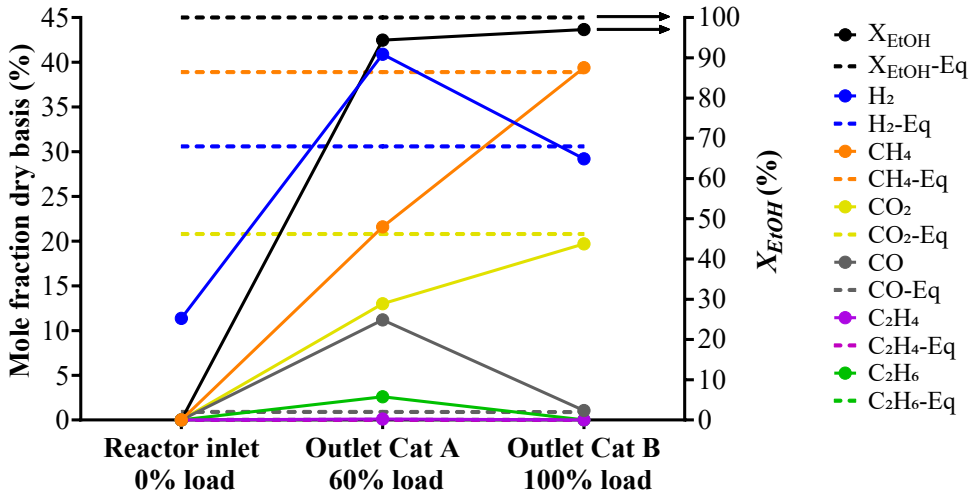

Figure 37. *Composition evolution along the pre-reformer using EtOH, 673 K, 0.5 MPag, GHSV 4200 h^{-1} and S/C 2*

There was no presence of products at the inlet of the reactor besides H_2, that as mentioned, it was intentionally added in the inlet stream to simulate a recycle that is normally used in the SR process to promote more H_2 production and reduce the possible influence of coke-forming reactions. The product distribution at the outlet of Cat A was rich in H_2, followed by CH_4, then an almost equimolar composition of CO and CO_2 near the 13% fraction; finally, 2.6% of ethane was detected. It was noticed that the product distribution at the outlet of Cat B section changed compared to the section of Cat A, indicating the possible predominance of other reactions towards higher CH_4 selectivity.

The final concentrations and the X_{EtOH} were almost identical to the ones predicted by the equilibrium in HYSYS® differing on average by 1% for CH_4, 5% for H_2 and CO_2, C_2H_4 was not detected while C_2H_6 measured 0.004% compared to the 0% predicted in the equilibrium. Therefore, it was possible to affirm that the equilibrium was reached considering that intermediate products like C_2H_4 and C_2H_6 were present only in traces as suggested in [23]. Again, this confirms the outstanding performance of the PR.

The elemental mass balances for C, H and O were solved considering the known total inlet flowrates for each species and the outlet dry gas stream flowrates calculated from the $\dot{F}^{out}$ and the compositions measured with the gas chromatograph. Considering this results, the overall experimental reaction is shown in Rx. 7 for the PR at *GHSV* 4200 h^{-1} and *S/C* 2 which can be interpreted as the total amount of EtOH, and H_2O consumed to actually form the measured products.

$$7C_2H_6OH + 5H_2O \leftrightarrows 10CH_4 + 6H_2 + 5CO_2 + 0.21CO + 0.001C_2H_6 \qquad \text{Rx. 7}$$

As mentioned in previous sections, the reaction pathway depends on many factors like *T*, *P*, *GHSV*, *S/C*, the properties of the catalysts, among others; several reactions might occur in series and/or in parallel making the EtOH steam pre-reforming an overall complicated reaction network [26]. Despite that a consensus about the reaction network has not been accomplished, there has been some agreements about the possible reactions that could proceed [24]. The mechanistic study for this report started with a literature review to determine the most common reactions proven to take place at the set experimental conditions, the information was summarized in Table 17.

Table 17. *Possible chemical reactions reported in literature for catalytic EtOH steam pre-reforming*

Name	Reaction	ΔH^0(kJ mol^{-1})	Rx. #
Complete EtOH SR	$C_2H_5OH + 3H_2O \leftrightarrows 2CO_2 + 6H_2$	173.5	Rx. 1
EtOH partial reforming 1	$C_2H_5OH + H_2O \leftrightarrows 2CO + 4H_2$	255.9	Rx. 8
EtOH partial reforming 2	$C_2H_5OH + 2H_2O \leftrightarrows 2CH_4 + H_2$	569.7	Rx. 9
Acetic acid formation	$C_2H_5OH + H_2O \leftrightarrows CH_3COOH + 2H_2$	41.8	Rx. 10
EtOH dehydrogenation	$C_2H_5OH \leftrightarrows CH_3CHO + H_2$	68.9	Rx. 11
Acetaldehyde decomposition 1	$CH_3CHO \leftrightarrows CH_4 + CO$	−18.9	Rx. 12
Acetaldehyde decomposition 2	$CH_3CHO + H_2O \leftrightarrows 3H_2 + 2CO$	186.9	Rx. 13
EtOH dehydration	$C_2H_5OH \leftrightarrows C_2H_4 + H_2O$	45.8	Rx. 14
EtOH dehydrative coupling	$C_2H_5OH \leftrightarrows \frac{1}{2}C_2H_5OC_2H_5 + \frac{1}{2}H_2O$	−11.9	Rx. 15
Polymerization	$C_2H_4 \rightarrow polymers \rightarrow 2C + 2H_2$	−52.5	Rx. 16
EtOH decomposition 1	$C_2H_5OH \leftrightarrows CO + CH_4 + H_2$	50.1	Rx. 17
EtOH decomposition 2	$C_2H_5OH \leftrightarrows \frac{1}{2}CO_2 + \frac{3}{2}CH_4$	−73.4	Rx. 18
EtOH decomposition 3	$C_2H_5OH \leftrightarrows \frac{1}{2}CH_3COCH_3 + \frac{1}{2}CO + \frac{3}{2}H_2$	70.9	Rx. 19
Methanation 1	$CO + 3H_2 \leftrightarrows CH_4 + H_2O$	−205.8	Rx. 5
Methanation 2	$CO_2 + 4H_2 \leftrightarrows CH_4 + 2H_2O$	−164.6	Rx. 20
Methane cracking	$CH_4 \rightarrow 2H_2 + C$	74.5	Rx. 21
Boudouard reaction	$CO \rightarrow \frac{1}{2}CO_2 + \frac{1}{2}C$	−86.2	Rx. 22
Water-gas-shift reaction	$CO + H_2O \rightarrow CO_2 + H_2$	−41.2	Rx. 6
CO reduction	$CO + H_2 \rightarrow C + H_2O$	−131.3	Rx. 23
CO_2 reduction	$CO_2 + 2H_2 \rightarrow C + 2H_2O$	−90.1	Rx. 24
Ethylene hydrogenation	$C_2H_4 + H_2 \leftrightarrows C_2H_6$	−137.1	Rx. 25
Ethylene SR	$C_2H_4 + 2H_2O \rightarrow 4H_2 + 2CO$	210.1	Rx. 26
Ethane SR	$C_2H_6 + 4H_2O \rightarrow 7H_2 + 2CO_2$	264.9	Rx. 27

Sources: [27, 61, 65, 66]

A thoughtful thermodynamic analysis reported by [61] used a Gibbs reactor to minimize the Gibbs free energy of the forementioned reactions to later calculate the reaction equilibrium constant in the range of (573 to 1473) K, a larger ln(K_{eq}) indicated more feasibility of occurrence. Based on this calculation, it was possible to determine the thermodynamic order of occurrence of the reactions at 673 K which was the T^{in} used for the experimental EtOH pre-reforming. The first list was defined in the following order:

Rx. # 18>12>17>1>5>25>20>13>8>19>14>23>26>24>22>6>10>15>27>11>21>9

To cut short the list of possible reactions, some of them were discarded supported by the evidence collected experimentally and in literature as follows:

The EtOH partial reforming 2 (Rx. 9) were discarded considering the thermodynamic analysis in [61] that determined it was not feasible at any *T*, whilst the Methane cracking (Rx. 21) was discarded because it was non-spontaneous at $T < 973$ K.

The Acetic acid formation (Rx. 10), EtOH dehydrative coupling (Rx. 15) and the EtOH decomposition 3 (Rx. 19) were discarded because the products of this reactions were not measured during the experiments and the purpose of this test was to determine a possible reaction network supported on experimental observations. Although they are feasible at 673 K, the occurrence of this reactions could not have been confirmed experimentally by the author.

Polymerization (Rx. 16), Boudouard reaction (Rx. 22), CO reduction (Rx. 23) and CO_2 reduction (Rx. 24) are coke-forming reactions, all of them feasible at the working conditions. However, coke was not detected after opening the PR during the experimental procedure even though C_2H_4 and C_2H_6 were present in the products after the Cat A section and several studies have shown that these compounds can be polymerized into gums [27], and later into carbon especially at T<673 K through the Boudouard reaction [26]. In this case, the concentration of H_2 in the inlet stream may have contributed to reduce the carbon polymer formation as proposed by [67]. Despite that some active metallic phases have shown enhanced stability over time with low coke formation [13], literature has proven that carbon deposition could not be yet definitely eliminated [17]. Being aware of this, it was decided to discard these reactions from the proposed reaction network since they might not have been noteworthy during the stability test, or the reaction rate was slow enough to avoid the significant formation of coke during the experiment time; nevertheless, in reality they might have happened.

Finally, the complete EtOH SR (Rx. 1) and the EtOH partial reforming 1 (Rx. 8) were discarded considering reports affirming that EtOH dehydrogenation, decomposition, and dehydration reactions can proceed much faster and occur before the SR reactions especially in the low *T* region [27].

After the previous statements, the list of thermodynamic possible order of reactions occurrence was shortened as follows:

RX. # 18>12>17>5>25>20>13>14>26>6>27>11

Considering this final list, the reaction network in Figure 38 (Next page) was proposed by the author. As expected, this mechanism showed several reactions occurring in series and/or parallel that could explain the obtained experimental results starting from the upstream reactants EtOH and water in presence of a simulated recycled H_2, all the way downstream to the main products H_2, CH_4, and CO_2. Additionally, based on the results, some mayor routes were proposed for each section of the PR that could explain the composition and the *T* profiles observed during the initial long-run stability test (Figure 30). The sign between brackets after the reaction number indicates whether the reaction is endothermic (+) or exothermic (−) based on the reaction enthalpies reported in Table 17.

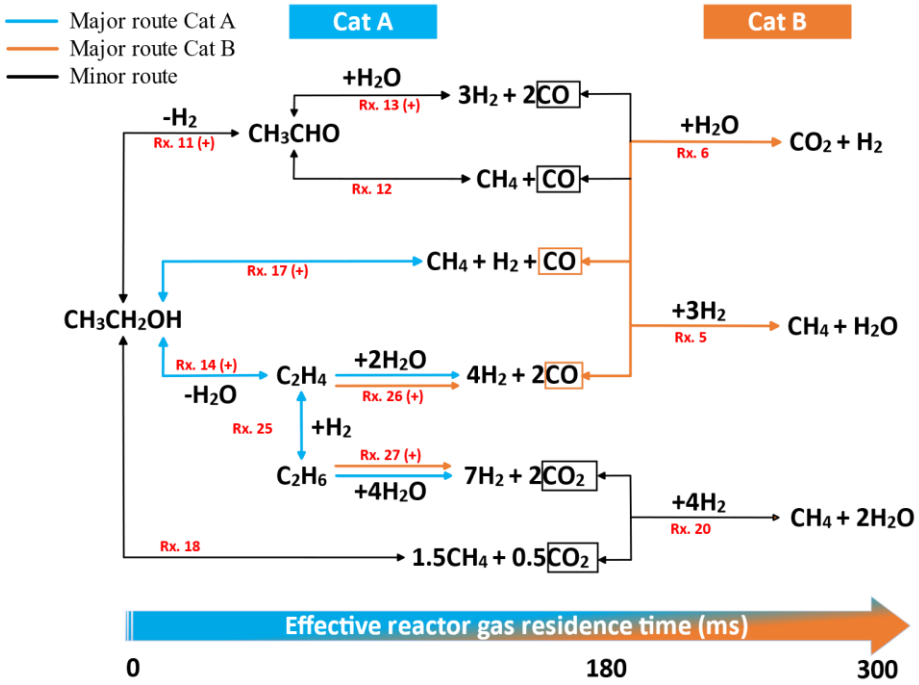

Figure 38. *Proposed reaction network for EtOH steam pre-reforming using Cat A and Cat B, 673 K, 0.5 MPag, 4200 h^{-1}, S/C 2.*

The composition and the *T* profiles observed during the tests suggested a dependency on the residence time, this result agreed with the reaction mechanism proposed by [68] where the authors demonstrated that breaking down reactions of EtOH took place first followed by the methanation and Water-gas-shift reactions. Some supporting arguments are presented below according to a detailed analysis of each reactor section proving the hypothesis that the reaction network presented in Figure 38 can potentially represent the behavior of the PR shown in Figure 37.

Cat A Section

- The 94% X_{EtOH} achieved with high selectivity towards H_2 production can be explained by the occurring reactions before the 180 ms t_{er} residence time mark where EtOH was broken down by at least four different reaction routes while H_2 was the main product especially from the SR reactions of intermediate hydrocarbons.
- The EtOH decomposition reactions (Rx. 17 and Rx. 18) were the most feasible based on the thermodynamic screening of reactions at the experimental conditions and could be the responsible for the CH_4 formation. Also, these reactions were proven to be feasible experimentally in a study published by [69] where 13.42% X_{EtOH} was calculated in a blank reactor at 673 K as consequence of EtOH thermal decomposition but considering that its occurrence in a catalytic reaction depends on the support and the characteristics of the active phase [64].
- The route of EtOH dehydration (Rx. 14) was confirmed experimentally by the presence of C_2H_4 as intermediate after the Cat A section, this reaction has been also reported in literature [26, 27] due to the C–O bond cleavage of EtOH over the catalyst's surface [28].
- The presence of C_2H_6 was also confirmed experimentally, this intermediate could have been result of the C_2H_4 hydrogenation reaction (Rx. 25) [65] that could have been favored considering the notable concentration of H_2 at the inlet of the reactor [27].

- It has been reported that the dehydration route could be extremely slow at low *T* [26], this could justify the presence of intermediate hydrocarbons detected experimentally even after 180 ms of reaction time.
- Since coke deposits were not noticed experimentally, the SR reactions of C_2H_4 (Rx. 26) and C_2H_6 (Rx. 27) could explain the consumption of the intermediate hydrocarbons. Additionally, 11 mol of H_2, 2 mol of CO and 2 mol of CO_2 could have been obtained from 1 mol of C_2H_4 and 1 mol of C_2H_6, this can be the explanation of the high H_2 content after Cat A section and the equimolar ratio of CO and CO_2 in the products.
- The EtOH dehydrogenation route (Rx. 11) has been extensively reported in literature as the main route for H_2 production at low *T* via the cleavage of O–H bonds followed by the C–C bond scission and decomposition of CH_3CHO into end products [23, 26–28]. It is characterized by a rapid formation and further consumption of CH_3CHO, especially this intermediate was not detected after 623 K [23, 26]. Nevertheless, this route was considered as minor for the proposed mechanism considering that it had the lowest thermodynamic favorability based on the cut-shorted list of possible reactions and that the presence of H_2 at the inlet of the reactor might have shifted the equilibrium constant back to EtOH instead of CH_3CHO promoting the C_2H_4 hydrogenation route instead as it was demonstrated experimentally.
- Finally, it should be remarked that six out of the nine governing reactions proposed for the Cat A section are endothermic compared to only three exothermic reactions; thus, Cat A section is expected to have predominantly endothermic behavior. This totally explains the experimental *T* profile registered in Figure 30 and Figure 43 where *T* dropped from 673 K at the inlet until reaching a minimum of 622 K at around 40% of the reactor load.

Cat B Section

- The X_{EtOH} increased from 94% to 97% after the Cat B section indicating that still some EtOH broke down into other compounds assumably by the same reaction routes proposed for the Cat A section; however, the small increase in conversion suggest that these reactions were not dominant for this section of the reactor.
- The composition profile of the Cat B section can be explained mainly by the methanation 1 (Rx. 5) and Water-gas-shift (Rx. 6) reactions occurring from the 180 ms to the 300 ms t_{er} residence time mark in which CO was exhausted completely with 82% increase of the CH_4 composition compared to the one reported after the Cat A section; the consumption of H_2 and the increase of CH_4 can be attributed to the methanation 1 reaction [23] whilst the symmetric variation of CO consumption and consequent CO_2 increase can be associated to the Water-gas-shift reaction [26, 70]. These reactions have been proven to run simultaneously in the same *T* range (573 to 723) K [26].
- Although the methanation 2 (Rx. 20) reaction was feasible, it was considered as a minor route since it involved CO_2 consumption, and this was not the representative behavior identified for the Cat B section where CO_2 increased until reaching the expected thermodynamic equilibrium composition.
- The intermediate hydrocarbons from the Cat A section were detected experimentally only as traces after the Cat B section; therefore, confirming that the SR reactions of C_2H_4 (Rx. 26) and C_2H_6 (Rx. 27) might also have occurred. Likewise, this intermediates are thermodynamically unstable with respect to the mixture of H_2, CO_2, CO and CH_4 [27]; therefore, the presence of these species only as traces were expected since it has been said that the PR reached experimental equilibrium conditions.

- At last, similar to the Cat A section, the experimental *T* profiles registered in Figure 30 and Figure 43 can also be explained by the predominant reactions proposed for the Cat B section of the pre-reactor. Methanation and Water-gas-shift reactions are highly exothermic [23] which can explain the *T* increase from the predominant endothermic region of Cat A to the exothermic region of Cat B within the reactor.

The proposed reaction network ends in the Cat B section with an expected 1 mol-H_2, 1 mol-CO_2, and 2 mol-CH_4. Comparing this to the overall experimental reaction defined in Rx. 7, the CH_4/H_2 ratio determined experimentally was 1.6 while the expected was 2; the experimental CH_4/CO_2 ratio was 2 which matched perfectly to the proposed final ratio of the mechanism; finally, the H_2/CO_2 experimental ratio was 1.2 compared the proposed theoretical of 1. It should be noticed also that experimentally unreacted C_2H_6 was detected which could mean that the stream needed more residence time to fully convert it and reach a fully thermodynamic equilibrium expecting an increase of H_2 and CO_2. Regardless of the differences, as an initial approach to describe a complex system, this proposed mechanism worked just fine to understand the evolution of the composition profiles in the PR.

In summary, considering the experimental observations supported by literature review, some general conclusions were addressed for this exploratory mechanistic study objective:

It can be affirmed that the reaction network proposed in Figure 38 may describe the behavior of the EtOH steam PR shown in Figure 37 operating at 4200 h^{-1} and *S/C* 2.

Cat A had selectivity towards H_2 while Cat B had it towards CH_4. This is possible since several studies have demonstrated this behavior using catalysts with different active phases and supports in the range of (573 to 723) K [26, 27, 64]. Additionally, this can be confirmed because the catalyst shared the same support but different active phases, and in general it has been proven that the nature of metal highly affect the final product distributions [64].

Even though some reactions were thermodynamically favored, the change of the product distributions at each catalytic section of the PR also proved that major routes might become minor and vice-versa determined by the nature of the catalyst [23, 24, 27].

In the low *T* region, H_2 and CO_2 are thermodynamically unstable with respect to CH_4 and H_2O; thus, At T<780 K CH_4 is the main product at equilibrium conditions. This is mainly due to the equilibrium of the methanation reaction and could be amplified when working at higher *P* [23, 27, 28].

The balance of the chemical reactions under specific operating conditions determines whether the overall reaction is endothermic or exothermic; hence, determining the *T* profile along the PR [62].

4.3. Experimental performance of the pre-reformer using Bioethanol

This final section validates the use of BioEtOH in the PR at the best operating conditions of *GHSV* 4200 h^{-1}–*S/C* 2.

4.3.1. Bioethanol short-run test

A short-run test similar to the ones conducted for the DOE study was done using the best selected conditions of *GHSV* 4200 h^{-1}–*S/C* 2 to have a first conclusion about the performance of the PR using real BioEtOH and comparing it to the values reported for Exp 2 in Table 8 of the DOE. Figure 39 and Figure 40 present the calculated values of the same

response variables that were discussed for the DOE and the initial long-run stability tests (Eq. 10 to Eq. 14). At first sight, the behavior of the PR using BioEtOH followed the same pattern as EtOH which was extensively discussed in previous sections of this report for all five performance variables.

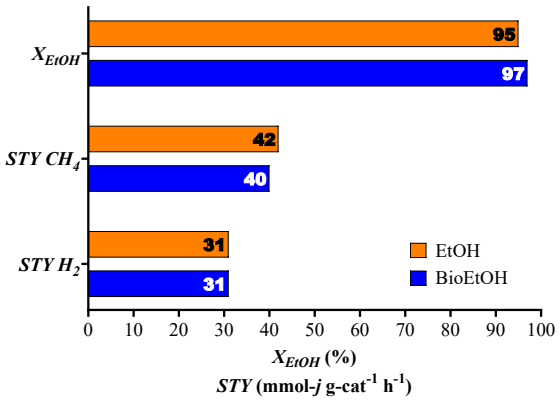

Figure 39. *Average value for X_{EtOH} and STY for the short-time test EtOH vs BioEtOH at 4200 h^{-1}, S/C 2*

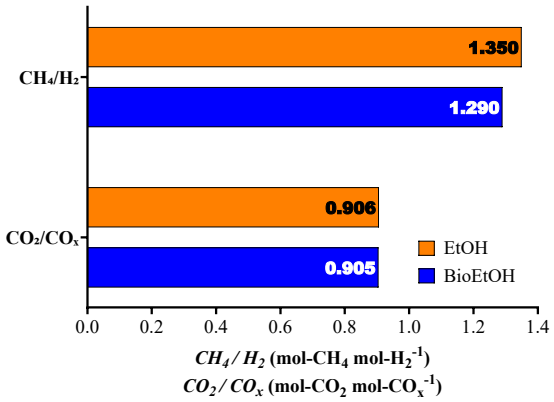

Figure 40. *Average value for product distribution and selectivity for the short-time test EtOH vs BioEtOH at 4200 h^{-1}, S/C 2*

Hypothesis tests were conducted to properly determine if the PR working with BioEtOH would perform equally as when it was operating with EtOH, the results are shown in Table 18. The results of all the SW tests had *p*-values > 0.05 indicating that for all parameters there was not enough evidence to reject H0; therefore, the samples might be considered normally distributed. The BF test *p*-values were all greater than 0.05 for all five groups meaning that there was not enough evidence to reject H0 and the variances could be considered equal. This was important to determine because it proved that all the criteria needed to properly do a *t*-test were met.

Table 18*. Hypothesis test to compare the short-run test performance of EtOH and BioEtOH*

	EtOH SW	**EtOH *p*-value SW**	**BioEtOH SW**	**BioEtOH *p*-value SW**	**BF**	**BF *p*-value**	***t***	***p*-value *t***
X_{EtOH}	1.0	0.9	0.9	0.3	1.8	0.2	-1.4	0.2
STY H_2	1.0	0.8	1.0	0.8	0.1	0.7	-0.4	0.7
STY CH_4	1.0	0.9	1.0	0.8	0.1	0.7	2.3	0.03[a]
$\frac{CO_2}{CO_x}$	0.9	0.2	0.9	0.4	0.1	0.8	1.2	0.2
$\frac{CH_4}{H_2}$	1.0	1.0	1.0	0.9	0.004	1.0	7.1	<0.001[a]

[a] Statistically significant at *p*-value ≤ 0.05

The student *t*-test demonstrated that there were not statistically significant differences for the response variables of X_{EtOH}, *STY* H_2, and CO_2/CO_x. In contrast, with *p*-value $t \leq 0.05$ statistically significant differences were identified between the performance of the pre-reactor using BioEtOH for *STY* CH_4 and CH_4/H_2.

This difference could be attributed to a slightly increased selectivity of BioEtOH to produce H_2 which also decreased the *STY* CH_4. This phenomenon had been reported in literature highlighting that the presence of other alcohols from fermentation like methanol and several higher C1–C5 alcohols isomers can be present in a real 2nd generation BioEtOH modifying

the reaction pathways [15]. For example, a study conducted by [16] showed that the presence of methanol and butanal increased the conversion and H_2 yield compared to pure synthetic EtOH. However, the BioEtOH used for the experiments in this work was highly pure (99.641% wt.) and its detailed traces composition was not known due to a confidentiality agreement; therefore, this hypothesis could not be confirmed but at the same time could not be discarded. Despite there were statistically significant differences in two out of five variables, they had little practical significance considering that the difference of *STY* CH_4 is only 5% between the mean values [71]. No coke formation was detected when using BioEtOH.

Based on this first comparison, the short-run test evidenced that the reactor with a loading of 60% Cat A, 40% Cat B, *GHSV* 4200 h^{-1} and *S/C* 2 performed similarly when working with EtOH and real BioEtOH.

4.3.2. Bioethanol long-run stability test

The long-run stability-test was the last and probably the most important test to determine if the reactor in the selected conditions was suitable for the pre-reforming of real BioEtOH. Figure 41 and Figure 42 show the progress of the discussed performance variables (Eq. 10 to Eq. 14) using BioEtOH and comparing it by the results obtained during the initial long-run stability test using EtOH at 4200 h^{-1}–*S/C* 2.

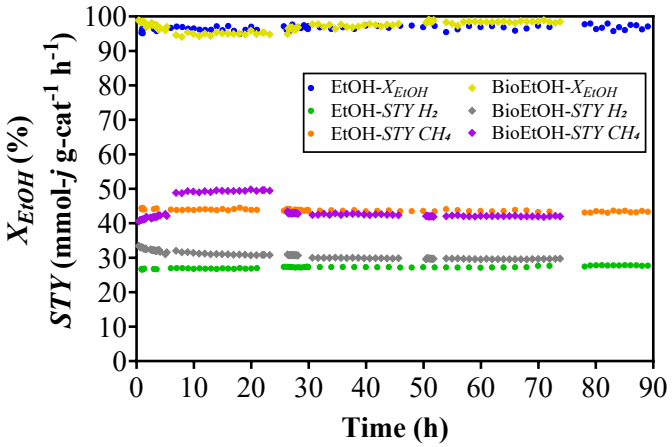

Figure 41. *X_{EtOH} and STY for the long-run stability test EtOH vs BioEtOH at 4200 h^{-1}, S/C 2*

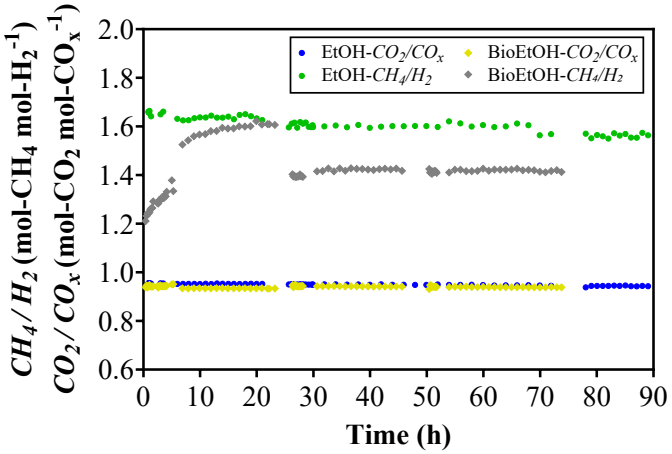

Figure 42. *Product distribution for the long-run stability test EtOH vs BioEtOH at 4200 h^{-1} - S/C 2*

Same as determined during the short-time test, the profile for X_{EtOH}, and CO_2/CO_x were also equal for EtOH and BioEtOH during the long-run stability test. However, differences were noted for the other three variables.

The jump on the data series for BioEtOH between (7 to 23) h was the result of decreasing the feed stream from *S/C* 2 to 1.5. Regardless of this change, the only noticeable effect was the increase of the CH_4/H_2 ratio and consequently an increase of the *STY* CH_4; this response agreed to the expected behavior as it was proven during the DOE experiment stage (Figure 22 and Figure 26). After the 23 h mark, the PR went back to the previous steady condition showing that it can tolerate fluctuations during the operation.

The average *STY* CH_4 for BioEtOH when working at *S/C* 2 was 4% lower compared to EtOH; in contrast, the average *STY* H_2 for BioEtOH was 12% higher compared to EtOH. Accordingly, the CH_4/H_2 distribution for BioEtOH was 12% lower than the one for EtOH. The inverse response of the distribution between these compounds were the same as discussed in previous sections, an increase of H_2 resulted in decreasing the amount of CH_4.

In this test, BioEtOH produced more H_2 than with EtOH, the reason could be the possible presence of impurities as described in the short-time test; but again, it could not be confirmed. Another reason could have been a difference of the packing protocol when loading the reactor that might have influenced the fluid dynamics and consequently mass transfer phenomena inside, although this could not be proved experimentally either. No coke formation was identified after the test.

The *T* profiles along the PR were plotted in Figure 43 using the average values when working at *S/C* 2 showcasing that EtOH and BioEtOH had the same profile; thus, providing more evidence that BioEtOH could be used in the catalytic PR at the selected conditions. The endothermic and exothermic profiles followed the same tendency as the ones obtained in the initial long-run stability tests (Figure 30) which behavior was also explained in the exploratory mechanistic study section.

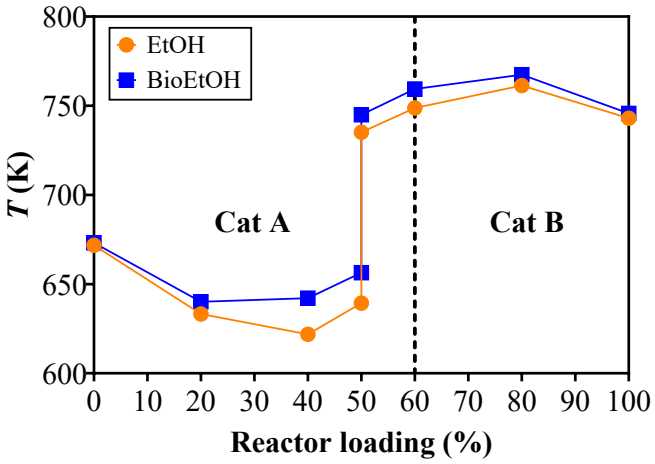

Figure 43. *T profile along the reactor during the stability test using EtOH and BioEtOH, 4200 h^{-1}, S/C 2*

Based on the detailed results of the long-term stability test comparing EtOH and BioEtOH, it was concluded that the PR with a loading of 60% Cat A, 40% Cat B, *GHSV* 4200 h^{-1} and *S/C* 2 performed the similarly when working with EtOH and the tested real BioEtOH.

CONCLUSIONS

This master's thesis assessed the technical feasibility of using real BioEtOH in the pre-reforming stage of a SR process for H_2 production using a reactor loaded with 60% Cat A and 40% Cat B and variable conditions of *GHSV* (2500 to 4200) h^{-1} and *S/C* (2 to 3.5). The achievement of the main goal was demonstrated by the successful completion of three specific objectives related to the study of the steady-state catalytic performance of the PR at different operating conditions using synthetic EtOH; by explaining the behavior of the reactor based on an exploratory reaction mechanistic study; and by the comparison of the performance when working with BioEtOH. The main findings were:

- The process variables of *GHSV* and *S/C* had an effect on the overall performance of the reactor especially for the H_2, CH_4 yield and the distribution of this two compounds in the overall composition profile of each experiment, in general, lower values of *S/C* and higher values of *GHSV* can be related to higher productivities.
- Some differences were detected for the EtOH conversion when changing the *GHSV* and *S/C*; however, it was demonstrated that they had no significant industrial practical difference because for all tested conditions, a conversion of over 90% was achieved.
- The process variables *GHSV* and *S/C* had no significant effect on the composition distribution of CO and CO_2, this was demonstrated experimentally and confirmed theoretically.
- The profile inside the reactor showed a decrease of the *T* in the Cat A section followed by a *T* increase in the latter Cat B section operating with EtOH and BioEtOH. This is attributed to the dominant chemical reactions occurring at each section. Cat A section promoted the reforming endothermic reactions whilst Cat B section promoted the methanation and water-gas shift exothermic reactions.
- Based on a KPI created for this study (PSI), it was demonstrated that the conditions of *GHSV* 4200 h^{-1}–S/C 2 had higher positive productivity effects than negative environmental impacts; thus, it was selected as the best operating condition.
- A possible reaction network was proposed to explain the steady-state behavior of the PR showing that the endothermic dehydration pathway is preferred for the Cat A section of the reactor, while Cat B section promoted more exothermic reactions.
- The comparison of the PR performance showed no practical differences when working with BioEtOH compared to synthetic EtOH in the short-run test.
- The long-run stability test at *GHSV* 4200 h^{-1}–S/C 2 showed a 12% increase in the H_2 productivity working with BioEtOH compared to EtOH possibly related to traces of higher alcohols; nevertheless, it was concluded that no practical differences were detected and the use of BioEtOH is suitable for the long operation with negligible coke formation in the run time.

As a general conclusion, the main objective was met and now it is possible to confirm that it is technically feasible to use real BioEtOH in a steam pre-reforming stage for H_2 production using the proposed reactor configuration at the studied operating conditions defined by TR. This thesis results served TR to achieve some specific goals set for the SHINE-FLEET and ZEPPELIN projects. Also, the results provided a detailed insight about the steady-state performance of the PR operating with EtOH and BioEtOH that will be used by TR for the future scale-up and industrial commercialization of this greener technology, thus, contributing to the goal of becoming a carbon neutral world by 2050.

RECOMMENDATIONS FOR FUTURE WORK

Based on the results of this master's thesis and considering the goal of TR to scale up this technology, the following recommendations for future work were suggested:

- To perform pilot-scale tests using real BioEtOH at the best selected conditions *GHSV* 4200 h^{-1}–*S/C* 2, the results could be more adequate to do technical-economical evaluations.
- To study the PR as an integral reactor by doing experiments with different loading with a 10% step, this would picture a more detailed evolution of the composition profile and the conversion over the bedding.
- Consider the proposed reaction mechanism network to conduct a detailed kinetic study to obtain accurate kinetic models that can be used for computational simulations and scale-up calculations.
- Conduct long-run stability tests with duration beyond the ones performed in this work to identify any gradual changes in catalyst activity, selectivity, or product distribution that might occur over extended operation time.
- Although coke formation was not detected at the best operating conditions, a further analysis on the topic could help to predict the catalyst life at the selected conditions and provide valuable insights for further industrial applications.
- Perform laboratory tests using a broader range of *GHSV* and *S/C* that could increase the productivity considering the discussed effect of this variables over some the performance indicators like conversion, selectivity and product distribution.
- Evaluate the use of low purity BioEtOH at the selected conditions, lower energy and water consumption would be expected; however, the influence of the impurities like higher alcohols should be studied carefully to avoid significant coke formation.
- Investigate the PR's performance under dynamic conditions simulating real-world operational fluctuations like changing the feed composition, the inlet *T* or work by ON/OFF cycles.
- To test other catalysts that might have an enhanced selectivity towards H_2 and coke resistance without increasing the operational costs.
- To validate the use of catalysts from several manufacturers, this will reduce the possible commercial dependence on a unique supplier and promote an open market competition for better price of acquisition and better customer/technical support. Additionally, it provides flexibility in case of a catalyst shortage from a supplier.
- Explore the integration of renewable energies like solar or wind at large scale to enhance the sustainability of H_2 production from BioEtOH.
- Start life cycle assessment studies to evaluate the impacts of using BioEtOH compared to conventional feedstocks for the pre-reforming process. This will determine the real sustainability impact and could provide information to obtain low-carbon emission H_2 certifications like CertifHy which could suppose a commercial advantage in the near future.

REFERENCES

[1] International Energy Agency. World Energy Outlook 2023, (2023). <https://iea.blob.core.windows.net/assets/86ede39e-4436-42d7-ba2a-edf61467e070/WorldEnergyOutlook2023.pdf> (accessed July 14, 2024).

[2] European Comission. The European Green Deal, Brussels, (2019). <https://eur-lex.europa.eu/resource.html?uri=cellar:b828d165-1c22-11ea-8c1f-01aa75ed71a1.0002.02/DOC_1&format=PDF> (accessed July 14, 2024).

[3] Hassan Q., Hafedh S.A., Mohammed H.B., Abdulrahman I.S., Salman H.M., Jaszczur M. A review of hydrogen production from bio-energy, technologies and assessments. Energy Harvesting and Systems 11 (2024). https://doi.org/10.1515/ehs-2022-0117.

[4] International Energy Agency. Global Hydrogen Review 2023, (2023). <https://iea.blob.core.windows.net/assets/ecdfc3bb-d212-4a4c-9ff7-6ce5b1e19cef/GlobalHydrogenReview2023.pdf> (accessed July 14, 2024).

[5] Franchi G., Capocelli M., De Falco M., Piemonte V., Barba D. Hydrogen Production via Steam Reforming: A Critical Analysis of MR and RMM Technologies. Membranes 10 (2020) 10. https://doi.org/10.3390/membranes10010010.

[6] International Energy Agency. Finland 2023 - Energy Policy Review, (2023). <https://iea.blob.core.windows.net/assets/07c88e41-c17b-4ea1-b35d-85dffd665de4/Finland2023-EnergyPolicyReview.pdf> (accessed July 14, 2024).

[7] International Energy Agency. Spain 2021 - Energy Policy Review, (2021). <https://iea.blob.core.windows.net/assets/2f405ae0-4617-4e16-884c-7956d1945f64/Spain2021.pdf> (accessed July 14, 2024).

[8] International Energy Agency. Colombia 2023 - Energy Policy Review, (2023). <https://iea.blob.core.windows.net/assets/2fa812fe-e660-42f3-99bc-bd75be3ca0b5/Colombia2023-EnergyPolicyReview.pdf> (accessed July 14, 2024).

[9] International Energy Agency. Poland 2022 - Energy Policy Review, (2022). <https://iea.blob.core.windows.net/assets/b9ea5a7d-3e41-4318-a69e-f7d456ebb118/Poland2022.pdf> (accessed July 14, 2024).

[10] Azizan M.T., Aqsha A., Ameen M., Syuhada A., Klaus H., Abidin S.Z., Sher F. Catalytic reforming of oxygenated hydrocarbons for the hydrogen production: an outlook. Biomass Conversion and Biorefinery 13 (2023) 8441–8464. https://doi.org/10.1007/s13399-020-01081-6.

[11] Jiménez-Llanos J., Ramírez-Carmona M., Rendón-Castrillón L., Ocampo-López C. Sustainable biohydrogen production by Chlorella sp. microalgae: A review. International Journal of Hydrogen Energy 45 (2020) 8310–8328. https://doi.org/10.1016/j.ijhydene.2020.01.059.

[12] de Abreu V.H.S., Pereira V.G.F., Proença L.F.C., Toniolo F.S., Santos A.S. A Systematic Study on Techno-Economic Evaluation of Hydrogen Production. Energies 16 (2023) 6542. https://doi.org/10.3390/en16186542.

[13] Palma V., Ruocco C., Cortese M., Martino M. Bioalcohol Reforming: An Overview of the Recent Advances for the Enhancement of Catalyst Stability. Catalysts 10 (2020) 665. https://doi.org/10.3390/catal10060665.

[14] Meloni E., Martino M., Iervolino G., Ruocco C., Renda S., Festa G., Palma V. The Route from Green H_2 Production through Bioethanol Reforming to CO_2 Catalytic Conversion: A Review. Energies 15 (2022) 2383. https://doi.org/10.3390/en15072383.

[15] Mokheimer E.M.A., Shakeel M.R., Harale A., Paglieri S., Mansour R. Ben. Fuel reforming processes for hydrogen production. Fuel 359 (2024) 130427. https://doi.org/10.1016/j.fuel.2023.130427.

[16] Le Valant A., Can F., Bion N., Duprez D., Epron F. Hydrogen production from raw bioethanol steam reforming: Optimization of catalyst composition with improved stability against various impurities. International Journal of Hydrogen Energy 35 (2010) 5015–5020. https://doi.org/10.1016/j.ijhydene.2009.09.008.

[17] Feng X., Zhao Y., Zhao Y., Wang H., Liu H., Zhang Q. A mini review on recent progress of steam reforming of ethanol. RSC Advances 13 (2023) 23991–24002. https://doi.org/10.1039/D3RA02769D.

[18] Fernández-Arias P., Antón-Sancho Á., Lampropoulos G., Vergara D. On Green Hydrogen Generation Technologies: A Bibliometric Review. Applied Sciences 14 (2024) 2524. https://doi.org/10.3390/app14062524.

[19] Lubbe F., Rongé J., Bosserez T., Martens J.A. Golden hydrogen. Current Opinion in Green and Sustainable Chemistry 39 (2023) 100732. https://doi.org/10.1016/j.cogsc.2022.100732.

[20] Adeli K., Nachtane M., Faik A., Saifaoui D., Boulezhar A. How Green Hydrogen and Ammonia Are Revolutionizing the Future of Energy Production: A Comprehensive Review of the Latest Developments and Future Prospects. Applied Sciences 13 (2023) 8711. https://doi.org/10.3390/app13158711.

[21] Ocenic E.-L., Tanţău A. Redefining the Hydrogen "Colours" based on Carbon Dioxide Emissions: A New Evidence-Based Colour Code. Proceedings of the International Conference on Business Excellence 17 (2023) 111–121. https://doi.org/10.2478/picbe-2023-0013.

[22] TÜV Rheinland. TÜV Rheinland Standard H2.21 Carbon-Neutral Hydrogen. (2021). <https://www.tuv.com/content-media-files/master-content/global-landingpages/images/hydrogen/tuv-rheinland-hydrogen-standard-h2.21_v1.0-en.pdf> (accessed July 23, 2024).

[23] Dalena F., Giglio E., Marino A., Aloise A., Giorgianni G., Migliori M., Giordano G. Steam Reforming of Bioethanol Using Metallic Catalysts on Zeolitic Supports: An Overview. Catalysts 12 (2022) 617. https://doi.org/10.3390/catal12060617.

[24] Silva J., Rocha C., Soria M.A., Madeira L.M. Catalytic Steam Reforming of Biomass-Derived Oxygenates for H_2 Production: A Review on Ni-Based Catalysts. ChemEngineering 6 (2022) 39. https://doi.org/10.3390/chemengineering6030039.

[25] Roldán R. Technical and economic feasibility of adapting an industrial steam reforming unit for production of hydrogen from renewable ethanol. International Journal of Hydrogen Energy 40 (2015) 2035–2046. https://doi.org/10.1016/j.ijhydene.2014.12.003.

[26] Kourtelesis M., Panagiotopoulou P., Ladas S., Verykios X.E. Influence of the Support on the Reaction Network of Ethanol Steam Reforming at Low Temperatures Over Pt Catalysts. Topics in Catalysis 58 (2015) 1202–1217. https://doi.org/10.1007/s11244-015-0485-7.

[27] Lin J., Chen L., Choong C.K.S., Zhong Z., Huang L. Molecular catalysis for the steam reforming of ethanol. Science China Chemistry 58 (2015) 60–78. https://doi.org/10.1007/s11426-014-5262-0.

[28] Zanchet D., Santos J.B.O., Damyanova S., Gallo J.M.R., Bueno J.M.C. Toward Understanding Metal-Catalyzed Ethanol Reforming. ACS Catalysis 5 (2015) 3841–3863. https://doi.org/10.1021/cs5020755.

[29] Nanda S., Rana R., Zheng Y., Kozinski J.A., Dalai A.K. Insights on pathways for hydrogen generation from ethanol. Sustainable Energy & Fuels 1 (2017) 1232–1245. https://doi.org/10.1039/C7SE00212B.

[30] Técnicas Reunidas S.A. Integrated report 2023, (2024). <https://www.tecnicasreunidas.es/wp-content/themes/tr/docs/informe-integrado-2024-EN.pdf> (accessed July 14, 2024).

[31] Técnicas Reunidas S.A. Short communication: Capital Markets Day, (2024). <https://www.tecnicasreunidas.es/es/wp-content/uploads/sites/3/2024/05/IP-Capital-Markets-Day-de-Tecnicas-Reunidas.pdf> (accessed July 14, 2024).

[32] Técnicas Reunidas S.A. TR leads the ShineFleet project, as a solution for hydrogen mobility of heavy vehicle fleets. (2021). <https://www.tecnicasreunidas.es/tr-leads-the-shinefleet-project-as-a-solution-for-hydrogen-mobility-of-heavy-vehicle-fleets/> (accessed July 14, 2024).

[33] Técnicas Reunidas S.A. ZEPPELIN Mission: circular economy at the service of green hydrogen production. (2022). <https://www.tecnicasreunidas.es/zeppelin-mission-circular-economy-at-the-service-of-green-hydrogen-production/> (accessed July 14, 2024).

[34] ASTM international. Designation: E29 − 22 Standard Practice for Using Significant Digits in Test Data to Determine Conformance with Specifications 1, USA, (2022). https://doi.org/10.1520/E0029-22.

[35] Cole T.J. Too many digits: The presentation of numerical data. Archives of Disease in Childhood 100 (2015) 608–609. https://doi.org/10.1136/archdischild-2014-307149.

[36] Mears D.E. Tests for Transport limitations in Experimental Catalytic Reactors. Ind. Eng. Chem. Process Des. Develop 10 (1971) 541–547. https://doi.org/https://doi.org/10.1021/i260040a020.

[37] Fogler H.S. Elements of Chemical Reaction Engineering, 4th ed., Pearson Education, Inc., Westford, USA, (2006).

[38] Worch E. 6.3 Fixed-Bed Process Parameters, in: Adsorption Technology in Water Treatment - Fundamentals, Processes, and Modeling, De Gruyter, (2012): pp. 176–178.

[39] Epstein N. On tortuosity and the tortuosity factor in flow and diffusion through porous media. Chemical Engineering Science 44 (1989) 777–779. https://doi.org/10.1016/0009-2509(89)85053-5.

[40] Rodrigues S.J., Vorhauer-Huget N., Richter T., Tsotsas E. Influence of Particle Shape on Tortuosity of Non-Spherical Particle Packed Beds. Processes 11 (2023). https://doi.org/10.3390/pr11010003.

[41] Chhabra R.B., Madivala G., eds. Flow of Fluids Through Granular Beds and Packed Columns, in: Coulson and Richardson's Chemical Engineering, 6th ed., Elsevier, (2019): pp. 335–386. https://doi.org/10.1016/B978-0-08-101098-3.00008-1.

[42] Coulson J.M. The flow of fluids through granular beds; effect of particle shape and voids in streamline flow. Transactions of the Institution of Chemical Engineers 27 (1949) 237–257.

[43] Hagen J. Industrial Catalysis, 2nd ed., WILEY-VCH Verlag GmbH & Co. KGaA, Weinheim, Germany, (2006).

[44] Bowden G.D., Pichler B.J., Maurer A. A Design of Experiments (DoE) Approach Accelerates the Optimization of Copper-Mediated 18F-Fluorination Reactions of Arylstannanes. Scientific Reports 9 (2019) 11370. https://doi.org/10.1038/s41598-019-47846-6.

[45] Jankovic A., Chaudhary G., Goia F. Designing the design of experiments (DOE) – An investigation on the influence of different factorial designs on the characterization of complex systems. Energy and Buildings 250 (2021) 111298. https://doi.org/10.1016/J.ENBUILD.2021.111298.

[46] Dastidar R.G., Galebach P.H., Lanci M.P., Wang C., Du Y., Huber G.W. Elucidation of reaction network and kinetics between cellulose-derived 1,2-propanediol and methanol for one-pot biofuel production. Green Chemistry 24 (2022) 350–364. https://doi.org/10.1039/d1gc03650e.

[47] Hone C.A., Kappe C.O. Towards the Standardization of Flow Chemistry Protocols for Organic Reactions. Chemistry-Methods 1 (2021) 454–467. https://doi.org/10.1002/cmtd.202100059.

[48] Ahmed H.E., Albolkany M.K., El-Khouly M.E., El-Moneim A.A. Tailoring MIL-100(Fe)-derived catalyst for controlled carbon dioxide conversion and product selectivity. RSC Advances 14 (2024) 13946–13956. https://doi.org/10.1039/d4ra01772b.

[49] Graschinsky C., Laborde M., Amadeo N., Le Valant A., Bion N., Epron F., Duprez D. Ethanol Steam Reforming over Rh(1%)$MgAl_2O_4$/Al_2O_3: A Kinetic Study. Industrial and Engineering Chemistry Research 49 (2010) 12383–12389. https://doi.org/10.1021/ie101284k.

[50] Llera I., Mas V., Bergamini M.L., Laborde M., Amadeo N. Bio-ethanol steam reforming on Ni based catalyst. Kinetic study. Chemical Engineering Science 71 (2012) 356–366. https://doi.org/10.1016/j.ces.2011.12.018.

[51] González A.G. Two level factorial experimental designs based on multiple linear regression models: a tutorial digest illustrated by case studies. Analytica Chimica Acta 360 (1998) 227–241. https://doi.org/10.1016/S0003-2670(97)00701-0.

[52] Montgomery D.C. 6 The 2k Factorial Design, in: Design and Analysis of Experiments, 9th ed., John Wiley & Sons, Inc., Hoboken, NJ, USA, (2017): pp. 230–307.

[53] Chen Y. On the analysis of unreplicated factorial designs, Doctoral thesis, University of Dortmund, 2003. <https://web.archive.org/web/20170809151216id_/https://eldorado.tu-dortmund.de/bitstream/2003/2777/1/Chenunt.pdf> (accessed July 5, 2024).

[54] Monteith E.R., Mampuys P., Summerton L., Clark J.H., Maes B.U.W., McElroy C.R. Why we might be misusing process mass intensity (PMI) and a methodology to apply it effectively as a discovery level metric. Green Chemistry 22 (2020) 123–135. https://doi.org/10.1039/c9gc01537j.

[55] Martínez J., Cortés J.F., Miranda R. Green Chemistry Metrics, A Review. Processes 10 (2022). https://doi.org/10.3390/pr10071274.

[56] Rossetti I., Compagnoni M., Torli M. Process simulation and optimization of H_2 production from ethanol steam reforming and its use in fuel cells. 2. Process analysis and optimization. Chemical Engineering Journal 281 (2015) 1036–1044. https://doi.org/10.1016/j.cej.2015.08.045.

[57] de Souza T.A.Z., Rocha D.H.D., Julio A.A.V., Coronado C.J.R., Silveira J.L., Silva R.J., Palacio J.C.E. Exergoenvironmental assessment of hydrogen water footprint via steam reforming in Brazil. Journal of Cleaner Production 311 (2021) 127577. https://doi.org/10.1016/j.jclepro.2021.127577.

[58] Alotaibi M.M., Alturki A.A. Optimizing Renewable Energy Integration for Sustainable Fuel Production: A Techno-Economic Assessment of Dimethyl Ether Synthesis via a Hybrid Microgrid-Hydrogen System. Fuels 5 (2024) 176–209. https://doi.org/10.3390/fuels5020011.

[59] Ferreira S.L.C., Caires A.O., Borges T. da S., Lima A.M.D.S., Silva L.O.B., dos Santos W.N.L. Robustness evaluation in analytical methods optimized using experimental designs. Microchemical Journal 131 (2017) 163–169. https://doi.org/10.1016/j.microc.2016.12.004.

[60] Compagnoni M., Tripodi A., Di Michele A., Sassi P., Signoretto M., Rossetti I. Low temperature ethanol steam reforming for process intensification: New Ni/M_xO–ZrO_2 active and stable catalysts

prepared by flame spray pyrolysis. International Journal of Hydrogen Energy 42 (2017) 28193–28213. https://doi.org/10.1016/j.ijhydene.2017.09.123.

[61] Tahir M., Mulewa W., Amin N.A.S., Zakaria Z.Y. Thermodynamic and experimental analysis on ethanol steam reforming for hydrogen production over Ni-modified TiO_2 /MMT nanoclay catalyst. Energy Conversion and Management 154 (2017) 25–37. https://doi.org/10.1016/j.enconman.2017.10.042.

[62] Fowles M., Carlsson M. Steam Reforming of Hydrocarbons for Synthesis Gas Production. Topics in Catalysis 64 (2021) 856–875. https://doi.org/10.1007/s11244-021-01496-z.

[63] Di Nardo A., Portarapillo M., Russo D., Di Benedetto A. Hydrogen production via steam reforming of different fuels: thermodynamic comparison. International Journal of Hydrogen Energy 55 (2024) 1143–1160. https://doi.org/10.1016/j.ijhydene.2023.11.215.

[64] Hou T., Zhang S., Chen Y., Wang D., Cai W. Hydrogen production from ethanol reforming: Catalysts and reaction mechanism. Renewable and Sustainable Energy Reviews 44 (2015) 132–148. https://doi.org/10.1016/j.rser.2014.12.023.

[65] Brus G., Tomiczek R.K.M., Mozdzierz M. Comparative study of two theoretical models of methane and ethane steam reforming process. Journal of Physics: Conference Series 745 (2016) 032151. https://doi.org/10.1088/1742-6596/745/3/032151.

[66] Yang L., Bukhovko M.P., Malek A., Li L., Jones C.W., Agrawal P.K., Davis R.J. Influence of Co on Ethylene Steam Reforming Over Co–Cr–O Spinel Catalysts. Catalysis Letters 151 (2021) 1456–1466. https://doi.org/10.1007/s10562-020-03396-5.

[67] Chen J. Hydrogen production in fixed-bed reactors with combined reformer-burner modules by steam-ethanol reforming at different temperatures. Authorea (2023). https://doi.org/10.22541/au.167569381.13621304/v1.

[68] Zhurka M.D., Lemonidou A.A., Anderson J.A., Kechagiopoulos P.N. Kinetic analysis of the steam reforming of ethanol over Ni/SiO_2 for the elucidation of metal-dominated reaction pathways. Reaction Chemistry & Engineering 3 (2018) 883–897. https://doi.org/10.1039/C8RE00145F.

[69] Therdthianwong A., Sakulkoakiet T., Therdthianwong S. Hydrogen Production by Catalytic Ethanol Steam Reforming. ScienceAsia 27 (2001) 193–198. https://doi.org/10.2306/scienceasia1513-1874.2001.27.193.

[70] Guerrero L., Castilla S., Cobo M. Advances in ethanol reforming for the production of hydrogen. Química Nova 37 (2014) 850–856. https://doi.org/10.5935/0100-4042.20140137.

[71] Cozby P.C., Bates S.C. 12 Understanding Research Results: Description and Correlation, in: Methods in Behavioral Research, 12th ed., McGraw-Hill Education, (2015): pp. 242–290.

LIST OF TABLES

Table 1. *Summary of chemicals and reactants used in the methodology* *18*
Table 2. *Summary of other materials used in the methodology* *18*
Table 3. *Summary of the equipment used in the methodology* *18*
Table 4. *Summary of software used in the methodology* *18*
Table 5. *Criterium used to define the number of significant digits for the reported values* *19*
Table 6. *Gas chromatography operating conditions* *22*
Table 7. *KPI's considered in the performance score* *27*
Table 8. *Calculated mean value of the DOE response variables* *30*
Table 9. *Curvature test results for the full factorial 2^2+center point DOE* *31*
Table 10. *ANOVA analysis of models to study the effect of GHSV and S/C on EtOH conversion* *31*
Table 11. *ANOVA analysis of models to study the effect of GHSV and S/C on STY H_2* *32*
Table 12. *ANOVA analysis of models to study the effect of GHSV and S/C on STY CH_4* *33*
Table 13. *ANOVA analysis of models to study the effect of GHSV and S/C on CO_2/CO_x ratio* *34*
Table 14. *ANOVA analysis of models to study the effect of GHSV and S/C on CH_4/H_2 ratio* *35*
Table 15. *Pre-reformer fluid dynamics parameters depending on GHSV* *36*
Table 16. *Calculated KPI values to select the best operating conditions based on stability tests* *42*
Table 17. *Possible chemical reactions reported in literature for catalytic EtOH steam pre-reforming* *45*
Table 18. *Hypothesis test to compare the short-run test performance of EtOH and BioEtOH* *50*

LIST OF FIGURES

***Figure 1**. H_2 use and summary map of announced low-emission hydrogen production projects by region. Source:[4]* 10
***Figure 2**. Classification of H_2 production based on colors. Source: [20]* 11
***Figure 3**. Bibliographic review of techno-economic evaluation of H_2 production from 1950 to 2023 based on color coding. Source: [18]* 12
***Figure 4.** Scheme of H_2 production technologies and their feedstock. Source: [12]* 12
***Figure 5.** Scheme of a SR process using a pre-reforming reactor. Source: [25]* 14
***Figure 6.** Possible reaction pathways for the BioEtOH pre-reforming process. Source: [29]* 15
***Figure 7.** Scheme of a SR process using a pre-reforming reactor. Source: [12]* 15
***Figure 8**. Experimental setup* 19
***Figure 9.** Process diagram of the experimental setup. Source: Author* 20
***Figure 10.** Reactor configuration for the EtOH steam pre-reforming using the Microactivity-Effi equipment setup. Source: Author* 21
***Figure 11.** Refractometer RX-5000, Atago CO., LTD. Source: Author* 22
***Figure 12.** Refractometer calibration curve for EtOH solutions (1 to 5) S/C ratio.* 22
***Figure 13.** Gas chromatograph process µGC, Agilent Technologies. Source: Author* 23
***Figure 14.** Full factorial 2^2 + 1 center point DOE surface.* 25
***Figure 15.** Graphical representation of the curvature test.* 26
***Figure 16.** EtOH pre-reforming simulation in Aspen HYSYS®* 29
***Figure 17.** Summary flowchart of the performed methodology.* 29
***Figure 18.** Interaction plot for EtOH conversion* 31
***Figure 19.** Response surface for EtOH conversion* 31
***Figure 20.** Interaction plot for STY H_2* 32
***Figure 21.** Response surface for STY H_2* 32
***Figure 22.** Interaction plot for STY CH_4* 33
***Figure 23.** Response surface for STY CH_4* 33
***Figure 24.** Interaction plot for CO_2/CO_x ratio* 34
***Figure 25.** Thermodynamic CO_2/CO_x distribution at different S/C. Source: [61]* 34
***Figure 26.** Interaction plot for CH_4/H_2 ratio* 35
***Figure 27.** Response surface for CH_4/H_2 ratio* 35
***Figure 28.** Output gas product distribution of the long-run stability tests at 673 K, 0.5 MPag* 37
***Figure 29.** EtOH pre-reforming product distribution as a function of T and S/C. Source: Author* 38
***Figure 30.** T profiles along the PR for the EtOH initial long-run stability test* 38
***Figure 31.** Evolution of EtOH conversion over time for the long-run stability tests at 673 K, 0.5 MPag* 39
***Figure 32.** Evolution of STY H_2 over time for the long-run stability tests at 673 K, 0.5 MPag* 40
***Figure 33.** Evolution of STY CH_4 conversion over time for the long-run stability tests at 673 K, 0.5 MPag* 40
***Figure 34.** Evolution of CO_2/CO_x over time for the long-run stability tests at 673 K, 0.5 MPag* 41
***Figure 35.** Evolution of CH_4/H_2 over time for the long-run stability tests at 673 K, 0.5 MPag* 41
***Figure 36.** PSI score given to each evaluated condition based on the KPI values* 42
***Figure 37.** Composition evolution along the pre-reformer using EtOH, 673 K, 0.5 MPag, GHSV 4200 h^{-1} and S/C 2* 44
***Figure 38.** Proposed reaction network for EtOH steam pre-reforming using Cat A and Cat B, 673 K, 0.5 MPag, 4200 h^{-1}, S/C 2.* 47
***Figure 39.** Average value for X_{EtOH} and STY for the short-time test EtOH vs BioEtOH at 4200 h^{-1}, S/C 2* 50
***Figure 40.** Average value for product distribution and selectivity for the short-time test EtOH vs BioEtOH at 4200 h^{-1}, S/C 2* 50
***Figure 41.** X_{EtOH} and STY for the long-run stability test EtOH vs BioEtOH at 4200 h^{-1}, S/C 2* 51
***Figure 42.** Product distribution for the long-run stability test EtOH vs BioEtOH at 4200 h^{-1} - S/C 2* 51
***Figure 43.** T profile along the reactor during the stability test using EtOH and BioEtOH, 4200 h^{-1}, S/C 2* 52